TUNNEL JUNCTIONS AS DETECTORS OF NOISE AND ENERGY RELAXATION IN SUPERCONDUCTING CIRCUITS

Andrey V. Timofeev

Dissertation for the degree of Doctor of Science in Technology to be presented with due permission of the Department of Applied Physics for public examination and debate in Auditorium AS1 at Helsinki University of Technology (Espoo, Finland) on the 3rd of Septemeber, 2009, at 12 o'clock noon.

ABSTRACT OF DOCTORAL DISSERTATION	HELSINKI UNIVERSITY OF TECHNOLOGY P. O. BOX 1000, FI-02015 TKK http://www.tkk.fi

Abstract

The experimental work presented in this Thesis addresses fundamental aspects of modern low temperature mesoscopic physics and nano-electronics. It focuses on noise and full counting statistics of electrical charge, and heat transport in superconducting circuits with sub-micron tunnel junctions. The Thesis summarizes the experiments on shot noise asymmetry, heat relaxation in a superconductor, and radiative electronic refrigeration, which are performed at sub-kelvin temperatures, when quantum phenomena of charge and energy transport take place.

The detailed mechanisms of electron transport in mesoscopic conductors can be revealed by studying their noise properties. Yet a sensitive noise detector with a broad bandwidth is required for a complete characterization of fluctuations. In this work, we employ a Josephson junction as an on-chip detector of shot noise and its non-Gaussian statistics in tunnel junctions. The detectable noise bandwidth is determined by the plasma frequency of the detector, which is about 50 GHz in our case. The non-Gaussian component of shot noise is related to the observed asymmetry of the switching rates of the Josephson junction when reversing the polarity of the noise current. The shot noise asymmetry is analyzed with the model of a non-resonant response of the detector to the third order fluctuations.

Thermalization and heat transport is an important issue to secure proper functioning of superconducting mesoscopic systems. We have investigated heat relaxation in a superconductor by injecting hot electrons into it and measuring the energy flux from electrons into phonons. The observations showed strong suppression of the flux at low temperatures, in qualitative agreement with the theory for clean superconductors. The quantitative comparison between the data and the theory suggests presence of an enhanced or additional energy relaxation mechanism.

Finally, we demonstrate the effect of remote electronic refrigeration in a superconducting circuit. We show that matching the circuit impedance enables refrigeration at a distance with a cooling power limited by the quantum of heat conductance. We also observe and analyze the crossover between electromagnetic and quasiparticle heat transport mechanisms in a superconductor. The observed effect can be applied to reduce harmful hot electron effects in mesoscopic devices operating close to the quantum limit.

Acknowledgments

The experimental work presented in this Thesis was carried out at the Low Temperature Laboratory at Helsinki University of Technology during 2004-2008 years. This Thesis could not have been realized without the support of many people whom I would like to thank.

First and foremost, I wish to express my gratitude to my supervisor, the leader of the PICO group Prof. Jukka Pekola, whose inspiring ideas, encouragement and instructive guidance stand behind this work. His help and advices have been invaluable during all these years. It has been an honour to work with such a dedicated scientist and outstanding team leader.

I would like to thank Dr. Matthias Meschke and Dr. Alexander Savin for the interesting discussions, invaluable help and many practical advices in the experimental aspects, especially at the early stage of this work.

It was a great pleasure to be a part of the PICO team, and I am grateful to the past and present members of the group with whom I had an opportunity to share excellent working atmosphere and also leisure times: Joonas Peltonen, Tommy Holmqvist, Meri Helle, Juha Muhonen, Sergey Kafanov, Sarah MacLeod, Ville Maisi, Antti Kemppinen, Olli-Pentti Saira, Juha Vartiainen and Mikko Möttönen.

It has been very pleasant and enjoyable to work and communicate with many great people in the Low Temperature Laboratory. Especially, I want to thank the past and present members of the lab for all the enlightening discussions: David Gunnarsson, Lorenz Lechner, Rob de Graaf, Anssi Salmela, Prof. Pertti Hakonen, Mika Sillanpää, Antti Paila, Romain Danneau, Wu Fan, René Lindell, Sorin Paraoanu, Alexander Sebedash and Vladimir Eltsov. I have also greatly benefited from the discussions with the theorists in the lab: Tero Heikkilä, Pauli Virtanen and Nikolai Kopnin. Many thanks to Rob Blaauwgeers and Pieter Vorselman from BlueFors company for the entertaining discussions and funny sauna evenings.

I thank the leader of the Low Temperature Laboratory Prof. Mikko Paalanen, who was always giving the moral support and encouragement throughout the whole Thesis. I would especially like to thank the secretaries of the Low Temperature Laboratory: Pirjo Muukkonen, Liisi Pasanen, Teija Halme, Tuire Koivisto and Leena Meilahti, for helping me with all of the administrative aspects during all these years.

I am grateful to Prof. Hervé Courtois and Prof. Erkki Lähderanta for the swift pre-examination of the manuscript. I wish also to thank Prof. Matti Kaivola for acting as a supervisor of this Thesis on behalf of the Department of Applied Physics.

I have had a great pleasure to work with our collaborators Francesco Giazotto and César Pasqual García, and I have also enjoyed valuable and interesting discussions with

Otaniemi, July 2009

Andrey Timofeev

Contents

List of publications

This thesis consists of an overview and of the following publications which are referred to in the text by their Roman numerals.

I A. V. Timofeev, M. Meschke, J. T. Peltonen, T. T. Heikkilä, and J. P. Pekola, *Wideband Detection of the Third Moment of Shot Noise by a Hysteretic Josephson Junction*, Phys. Rev. Lett. **98**, 207001 (2007).

II J. T. Peltonen, A. Timofeev, M. Meschke, and J. P. Pekola, *Detecting Current Noise with a Josephson Junction in the Macroscopic Quantum Tunneling Regime*, J. Low Temp. Phys **146**, 135 (2007).

III J. T. Peltonen, A. Timofeev, M. Meschke, T. T. Heikkilä, and J. P. Pekola, *Detecting non-Gaussian current fluctuations using a Josephson threshold detector*, Physica E **40**, 111122 (2007).

IV A. V. Timofeev, C. Pascual García, N. B. Kopnin, A. M. Savin, M. Meschke, F. Giazotto, and J. P. Pekola, *Recombination-Limited Energy Relaxation in a Bardeen-Cooper-Schrieffer Superconductor*, Phys. Rev. Lett. **102**, 017003 (2009).

V Andrey V. Timofeev, Meri Helle, Matthias Meschke, Mikko Möttönen, and Jukka P. Pekola, *Electronic Refrigeration at the Quantum Limit*, Phys. Rev. Lett. **102**, 200801 (2009).

Author's contribution

The research work presented in this Thesis has been carried out in the PICO group in the Low Temperature Laboratory at Helsinki University of Technology during 2004-2008 years. The author's main contribution included performing low temperature experiments and data analysis, as well as sample fabrication. The author carried out most of the measurements in publications I-III and a significant part of the measurements in publications IV and V. The author has also fabricated all of the samples for the experiments in publications I-III and the last of the two samples in publication V. The author carried out most of the data analysis in publications I, II, IV and V. In paper V, the author has also performed the modelling. The author has written the most part of publication V and participated in writing of publications I and IV.

In addition, the author has presented the results of this Thesis in a number of international physics schools, workshops and conferences including the ULTI Users Meeting on Quantum Phenomena at Low Temperatures in Lammi (Finland) 2006, the Workshop on Quantum Electromechanical Systems (QEM-2) in Morro Bay (California, USA) 2006, the European School on Nanosciences and Nanotechnology in Grenoble (France) 2007, the VIth Rencontres de Moriond in Mesoscopic Physics in La Thuile (Italy) 2008, the Conference on Micro- and Nano-cryogenics in Espoo (Finland) 2008, and The 25th International Conference on Low Temperature Physics in Amsterdam (the Netherlands) 2008.

Introduction and Thesis Overview

Mesoscopic nanophysics studies solid-state systems and conductors of small dimensions, typically of the order of a micron or smaller. The electrical and thermal properties of mesoscopic systems and based on them micro- and nano-devices are determined by the laws of quantum mechanics. This is due to the fact that wave nature of electrons and quantization of the electron charge become essential in the description of charge and heat transport at short length scales. A tunnel junction is a well-known mesoscopic object in which the wave nature of electrons manifests itself. The electrons can tunnel through a thin insulating barrier between two conducting electrodes of the junction, making electrical current flow possible through the junction. Another consequence of quantum mechanics is transition of a normal metal into a superconducting state at low temperatures. The electrons form so-called Cooper pairs in a superconductor, which carry current without dissipation. A superconducting tunnel junction, often known as a Josephson junction, has found many different applications in mesoscopic physics and cryogenic electronics, e.g. in single electron devices, in magnetic field sensors (SQUIDs) used in magnetoencephalography to study human brain, and as a building element for a yet-to-be-realized quantum computer. This Thesis is devoted to the experimental studies of charge and heat transport phenomena in superconducting circuits with tunnel junctions.

The basic information about charge transport properties of mesoscopic systems can be obtained from conductance measurements. However this information is far from complete. The quantization of the electron charge leads to the appearance of shot noise in mesoscopic conductors. The studies of shot noise reveal detailed mechanisms of electron transport in mesoscopic conductors, providing information about electron correlations and effective transferred charge, which is not obtainable from ordinary conductance measurements [1]. The recent theoretical advance such as full counting statistics (FCS) of electron charge [2, 3] gives a complete characterization of fluctuations in mesoscopic conductors, allowing to calculate any order charge correlations. However, to measure noise and verify the results of FCS in practice is a non-trivial task. Only fairly recently the first experiments on FCS have been performed [4], and this research field is rapidly developing, aiming towards measurements of frequency dependent high order correlations in various mesoscopic systems. Yet there is a need for a detector which could be used to measure shot noise and electron transport statistics at high frequencies. In this Thesis a Josephson junction is implemented as a wideband detector of shot noise and higher

order current fluctuations in tunnel junctions.

Thermalization and heat transport represent another important issue in mesoscopic systems, especially in superconducting structures. A mesoscopic system can be considered as two interacting subsystems, the electrons and the phonons (quantized vibrations of the atomic lattice), whose temperatures can differ in a general case. In a typical situation, when a mesoscopic structure is electrically biased, the electron temperature is usually higher than that of the phonon system. This may lead to hot electron effects which strongly influence and limit the performance of low temperature mesoscopic devices, in particular electronic refrigerators, thermometers and radiation detectors. The studies of heat relaxation mechanisms are essential to secure proper thermalization of the devices. At higher temperatures, the electron-phonon interaction is the basic mechanism of electron heat relaxation. At lower temperatures, when the atomic lattice is sufficiently cold, another electron energy relaxation mechanism due to electromagnetic radiation becomes dominant in small metallic structures. In this work both of the relaxation processes are investigated.

This Thesis includes the results of the experiments on three themes: on shot noise asymmetry, on heat relaxation in a superconductor, and on radiative electronic refrigeration. In all of the experiments, tunnel junctions are employed as sensitive detectors to study either charge or heat transport in superconducting and hybrid normal metal - superconductor structures.

The Thesis is organized as follows. Chapter 1 briefly discusses properties of superconductors and tunnel junctions. Chapter 2 describes the experimental aspects of the work. Chapter 3 is devoted to the experiments on shot noise. A Josephson junction is shown to be a sensitive detector to measure non-Gaussian statistics of electrical current in tunnel junctions. The influence of non-Gaussian noise on the detector dynamics is described with a model of a slow response to the third order fluctuations. Chapter 4 describes the experiments on energy relaxation in a superconductor. The electron-phonon heat flux in a superconductor is found to be suppressed with respect to that in the normal state, in a qualitative agreement with the theory of electron-phonon relaxation for clean superconductors. The quantitative comparison with the theory indicates that the energy relaxation also depends on additional, still to be investigated microscopic mechanisms. Chapter 5 is devoted to the experiments on radiative electronic refrigeration. A remote refrigeration of a metallic island is demonstrated with a cooling power limited by the quantum of thermal conductance. The relevance of circuit matching is shown experimentally. Also, the crossover between electromagnetic and quasipartcile heat transport is observed and analyzed. The Thesis conclusions and future prospects are discussed in Summary and Outlook.

Chapter 1

Basic characteristics of superconductors and tunnel junctions

According to the microscopic Bardeen-Cooper-Schrieffer theory [5], the superconducting state is formed of Cooper pairs of electrons due to a weak attractive interaction between the two electrons with opposite momenta and spins, coherently scattering on atomic lattice vibrations or phonons. The Cooper pairs are condensed in the ground state of the superconductor, and they can be described by a single macroscopic superconducting wave function $\psi(\mathbf{r}) = |\psi(\mathbf{r})|e^{i\phi(\mathbf{r})}$ with amplitude $|\psi(\mathbf{r})|$ and phase $\phi(\mathbf{r})$, where $|\psi(\mathbf{r})|^2$ represents the density of Cooper pairs. The single particle excitations are separated by the temperature dependent energy gap $\Delta(T)$ from the ground state. The energy gap vanishes at the critical temperature T_c, at which the transition between the superconducting and the normal state occurs. The density of single particle states with energies E in the ideal superconductor at zero temperature is given by:

$$N_s(E) = N(0)\frac{|E|}{\sqrt{E^2 - \Delta^2}}\theta(|E| - \Delta). \tag{1.1}$$

Here, $N(0)$ is the density of states in the normal metal state at the Fermi level E_F[1], and the Heaviside step function $\theta(x) = 1$ for $x \geqslant 0$ and 0 otherwise.

The conductance measurements of superconducting tunnel junctions allow one directly to investigate the energy gap and the density of states in superconductors, as it was first demonstrated in the pioneering experiments by Giaever and Megerle [7]. Also, certain characteristics of tunnel junctions show exponential dependence on bias current and on temperature, and therefore they can be used as very sensitive detectors for studying charge and heat transport in mesoscopic systems, as we discuss in more detail below.

---

[1]Throughout the Thesis, the energies of single particle excitations are given with respect to the Fermi energy E_F. For the aluminium, which is used in this work as a superconductor, $E_F \simeq 12$ eV, $N(0) \simeq 2 \cdot 10^{47}\text{J}^{-1}\text{m}^{-3}$, and the Fermi velocity $v_F \simeq 2 \cdot 10^6$ m/s [6]. For aluminium films, a typical measured value of the critical temperature is $T_c \simeq 1.4$ K and of the energy gap is $\Delta \simeq 0.2$ meV at temperatures below 0.4 K.

SIS junction

In a superconductor-insulator-superconductor (SIS) junction, a non-dissipative current of Cooper pairs can flow due to the interference between the wave functions of the two superconducting electrodes. The supercurrent $I_s(\varphi)$ depends on the phase difference φ across the tunnel barrier according to the DC Josephson relation $I_s(\varphi) = I_c \sin \varphi$. The critical current I_c determines the maximal non-dissipative current through the junction, showing how strong the superconducting electrodes are coupled to each other. The critical current is related to the tunnel resistance R_T and temperature T via the Ambegaokar-Baratoff relation $I_c = \dfrac{\pi \Delta}{2eR_T} \tanh \dfrac{\Delta}{2k_B T}$ [8]. When the current through the junction is larger than the critical current, a finite time-periodic voltage appears across the junction, and the phase difference evolves in time according to AC Josephson relation $d\varphi/dt = 2eV/\hbar$. The coupling energy of a SIS junction is determined by the Josephson energy $E_J = \hbar I_c/2e$. The phase dynamics of a Josephson junction depends on the relation between the Josephson energy E_J, charging energy $E_C = e^2/2C$ (C is the junction capacitance), and thermal energy $k_B T$, and it is also determined by the damping parameter, which depends on the admittance of the electromagnetic environment of the junction. An under-damped Josephson junction with $E_J > E_C$ has a hysteretic current-voltage characteristic — the junction switches from the superconducting to a normal state when the current through the junction reaches or exceeds the critical current I_c. Furthermore, the switching rate is exponentially sensitive to the bias current. The threshold property and high sensitivity to fluctuations make a Josephson junction to be used as a very sensitive detector to study shot noise, as discussed in detail in Chapter 3.

SIS junction can be also used as a thermometer to probe quasiparticle temperature in a superconductor by biasing the junction at sub-gap voltages $V < 2\Delta/e$. The current-voltage IV characteristic of such a junction has a sub-gap current plateau [9], whose height magnitude I depends almost exponentially on temperature according to

$$I = \frac{1}{eR_T} \int_{-\infty}^{\infty} dE n_s(T_1, E - eV) n_s(T_2, E)[f_{T_1}(E - eV) - f_{T_2}(E)]. \tag{1.2}$$

Here, f_{T_1} and f_{T_2} are the distribution functions, and $n_s(T_1)$ and $n_s(T_2)$ are normalized to $N(0)$ densities of states in the two superconducting electrodes at temperatures T_1 and T_2, correspondingly. In the equilibrium case, the electron distribution is described by the Fermi-Dirac function $f(E, T) = (1 + e^{E/k_B T})^{-1}$. This method of probing temperature with a SIS junction is used in the studies of energy relaxation in a superconductor in Chapter 4.

NIN junction

A IV-characteristic of a normal metal-insulator-normal metal NIN junction has no tem-

perature dependence and thus is ohmic in the limit of a very high tunnel barrier. There is a correction to this result due to a finite barrier height [10], which makes NIN junction suitable for thermometry in a wide temperature range (50-400 K in the experiments by Gloos *et al.* [11]). Yet a NIN junction can be also used as Coulomb blockade thermometer (CBT)[12]. The CBT is a primary thermometer, i.e. it requires no calibration — the thermometer signal depends on temperature only via fundamental constants. The operation principle is based on measuring the lowest order corrections in $E_C/k_B T$ to the junction conductance, which originates due to a weak Coulomb blockade, when $E_C \lesssim k_B T$. For a high precision thermometry, typically an array of few tens of NIN junctions in series is used where the fluctuations of a voltage bias are well suppressed [13, 14, 15]. The current-voltage characteristic of such an array of N tunnel junctions has no sharp Coulomb blockade gap, but it is smeared over a bias range $eV \sim N k_B T$. The voltage dependent conductance $G(V) = dI/dV$ of an array of N junctions with a charging energy E_C is related to temperature via [12]

$$\frac{G(V)}{G_T} = 1 - \frac{E_C}{k_B T} g\left(\frac{eV}{N k_B T}\right). \tag{1.3}$$

Here, G_T is the asymptotic conductance of the junction and function $g(x) = [x \sinh(x) - 4\sinh^2(x/2)]/[8\sinh^4(x/2)]$. The conductance correction (1.3) represents a bell-shaped symmetric curve around $V = 0$ (Fig. 1.1). In the limit $E_C \ll k_B T$ the width of $G(V)/G_T$
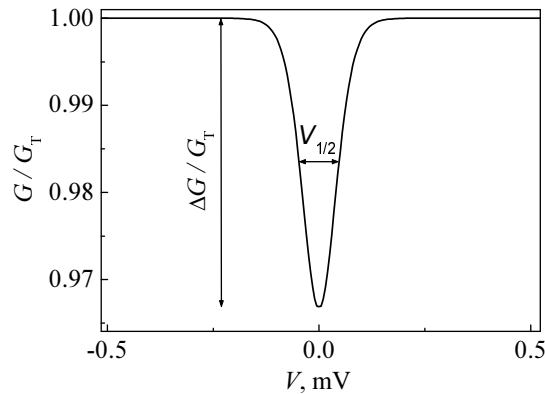
Figure 1.1: CBT conductance peak (1.3), calculated for $N = 2$ junctions with $E_C/k_B = 20$ mK at $T = 0.1$ K.

at half minimum is given by $V_{1/2} = 5.44 N k_B T$, which allows one to determine temperature straightforwardly without calibration. Also, the depth of the conductance minimum is inversely proportional to temperature as $\Delta G/G_T = E_C/(6 k_B T)$. The method of Coulomb blockade thermometry is used to investigate energy relaxation in the normal metal state in Chapter 4.

NIS junction

A normal metal-insulator-superconductor NIS junction can be used as a thermometer to probe the electron temperature T_e of the normal electrode [9]. The current through the NIS junction

$$I = \frac{1}{2eR_T} \int_{-\infty}^{\infty} dE n_s(E)[f(E - eV, T_e) - f(E + eV, T_e)]. \tag{1.4}$$

depends only on T_e. It is insensitive to the temperature of S-electrode as long as the superconducting gap almost equals to its zero temperature value, i.e. at temperatures $T \lesssim 0.3T_c$. In a case of low temperatures $k_B T_e \ll \Delta$, the current at voltages $0 \ll eV \ll \Delta$ can be approximated by $I(V) \simeq \frac{\Delta}{eR_T}\sqrt{\frac{\pi k_B T_e}{2\Delta}}e^{(eV-E)/k_B T_e}$ [16]. The IV characteristic of a thermometer becomes increasingly rounded with temperature increase as shown in Fig. 1.2. In typical experiments, the thermometer is biased with a small constant current
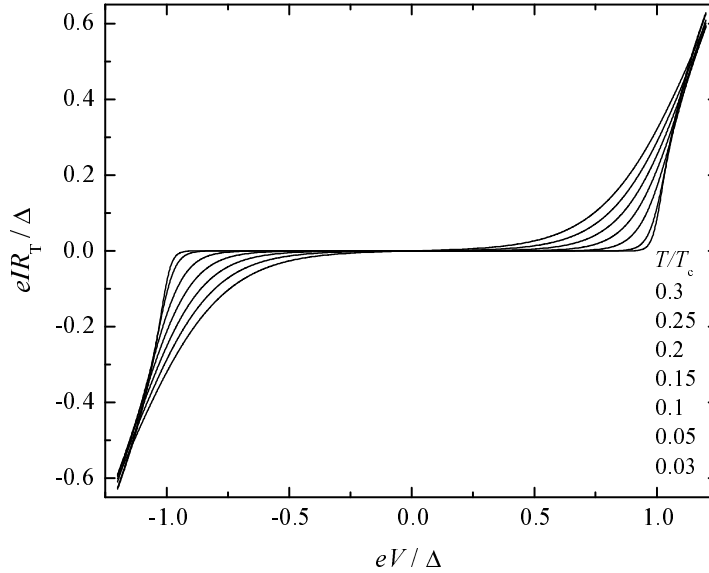
Figure 1.2: Calculated IV curves of a NIS junction at several temperatures, normalized to the critical temperature T_c.

(in pA range) to achieve high sensitivity, and one measures a temperature dependent voltage across the junction.

NIS junctions are also used in electronic refrigeration of the normal metal electrode [9, 17, 18]. The physical mechanism of the refrigeration is based on a selective tunneling of hot quasiparticles through the insulating barrier. When the junction is biased at voltages $|V| \lesssim \Delta/e$, only the quasiparticles with energies $E > \Delta$ can tunnel from the normal metal into the superconductor, since the states within the superconducting gap are forbidden. Thus, each tunneling electron removes energy of amount $E - eV$ from

the normal metal. The rate of the net heat flux in NIS junction is given by

$$\dot{Q} = \frac{1}{e^2 R_T} \int dE (E - eV) n_s(E)[f(E - eV, T_e) - f(E, T_e)]. \tag{1.5}$$

$\dot{Q}$ is positive at voltages $|V| < \Delta/e$, corresponding to the cooling of a normal metal, and the maximum of $\dot{Q}$ is achieved at $eV \approx \Delta$. At voltages $eV > \Delta$, $\dot{Q}$ is negative, and both the N and S electrodes are heated up. Using a SINIS structure doubles the cooling power, since the cold quasiparticles with energies $E < -\Delta$ are injected from the second superconducting electrode into the normal metal below the Fermi level. The SINIS structures are used both as electronic thermometers and refrigerators in the experiments on radiative heat transport described in Chapter 5.

Chapter 2

Experimental methods

The structures investigated in this work are made of thin metallic films (typically $20-100$ nm thick) of aluminium, copper, or gold-palladium, deposited on an oxidized silicon substrate with planar geometry design. They are fabricated with the standard methods of electron beam lithography and thin film shadow deposition (electron beam evaporation) techniques. A tunnel barrier can be formed by oxidation of aluminium film (AlOx) and its thickness is about 1-2 nm. The low frequency electrical measurements (up to 10 kHz) of the structures are carried out in a dilution refrigerator at temperatures 30 mK - 1 K. At these temperatures, the aluminium is used as a superconducting bottom junction electrode. Copper and gold-palladium are used as normal metal top electrodes of the junction. These techniques allow one to study electronic properties of the structures of desired planar geometry with superconductor-insulator-superconductor (SIS) or/and superconductor-insulator-normal metal (SIN) junctions (Fig. 2.1).

Sample fabrication

The samples were fabricated on an oxidized silicon wafer with the oxide thickness 300 nm. The first fabrication step was to form the mask of the desired geometry in the electron-sensitive resist by electron beam lithography. Two different resist layers were spun on top of the wafer. The bottom resist layer is a copolymer, a polymethyl-metacrylate-methacrylic acid (PMMA-MAA) dissolved in ethyl lactate (8%), which is used as a buffer support for the top resist layer. The function of the bottom layer is to give a sufficient undercut to allow for the shadow deposition. The copolymer was spun at 4000 rpm for 40 sec and baked on the hot plate at 170 - 180 °C for 15 min, which formed a resist layer with the thickness of about 200 - 300 nm. To form large area junctions > 1 μm^2, the latter step was repeated a few times to achieve the desired thickness (of about 1 μm) of the bottom resist. The top resist layer is polymethyl-metacrylate (PMMA) dissolved in anisole (3% solution), and it was spun at 2500 rpm and baked for 15 min. This final top resist layer is fairly robust to form suspended bridges and its thickness is $\sim$ 100 - 200 nm. After the electron beam exposure, which breaks the polymer chain structure of the resist, the sample is developed in methyl-isobutyl-ketone isopropanol

(MIBK-IPA) solution in 1:3 proportion for 20 - 60 sec and rinsed with isopropanol. The second main fabrication step was angle deposition of metallic films onto the sample in an ultra-high-vacuum chamber of the electron beam evaporator. The oxidation of aluminium film was done in the same chamber for 2 - 10 min at pressures 0.1 - 10 mbar. After the evaporation, the unexposed resist with covering metallic films is removed with a lift-off process in acetone.
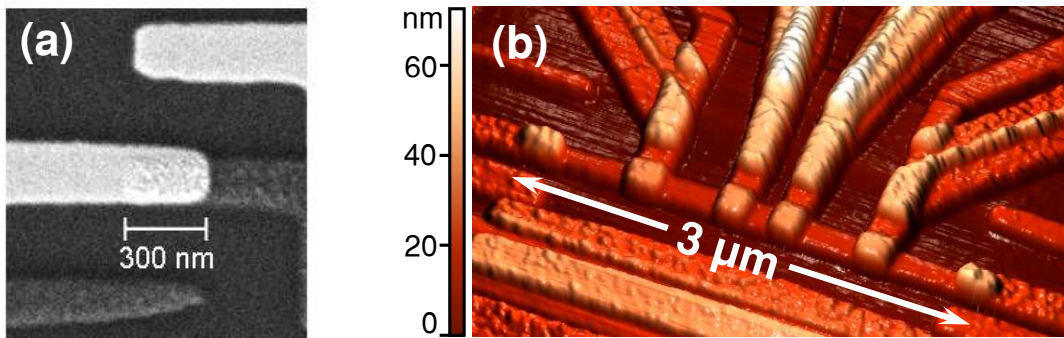
Figure 2.1: (a) A typical NIS junction (Al-AlOx-AuPd) fabricated by electron beam lithography and shadow evaporation. (b) Colored atomic force microscopy image of the gold palladium island, which is the part of the sample measured in the experiments on quantum electronic refrigeration, described in Chapter 5. The island is contacted by four NIS tunnel junctions (AuPd-AlOx-Al) in the middle and direct metal-to-metal contacts at the ends.

Measurement setup

The measurements were carried out in a ^{3}He - ^{4}He dilution refrigerator with a plastic heat exchanger, whose base temperature is about 30 - 50 mK. The sample chip with the formed structure was thermally anchored to the cryostat sample holder and electrically connected to it with ultrasonically bonded aluminium wires. The cryostat has 12 DC-signal lines and its electrical wiring scheme is shown in Fig. 2.2. The manganin twisted-pair wires are used for the connection between room temperature and the 1 K plate. The Thermocoax® lines between 1 K plate and 50 mK are of about 1 m long to provide sufficient attenuation of high frequency noise [19]. To suppress small inductively coupled noise, which may lead to large noise currents in the superconducting bonding wires and in the sample, we used surface mounting resistors of 220 Ω on the sample stage. For sample biasing, both commercial[1] and custom battery powered voltage sources were used. The bias voltages were attenuated and low-pass filtered at room temperature. The voltage across the sample was amplified by low noise differential pre-amplifiers[2]. The current was measured by DL-instrument 1211 current pre-amplifier.

---

[1] Agilent 33220A function generators and SRS DC SIM928 isolated voltage sources.
[2] HMS 568 electronik or DL-instrument 1201 differential voltage pre-amplifiers.
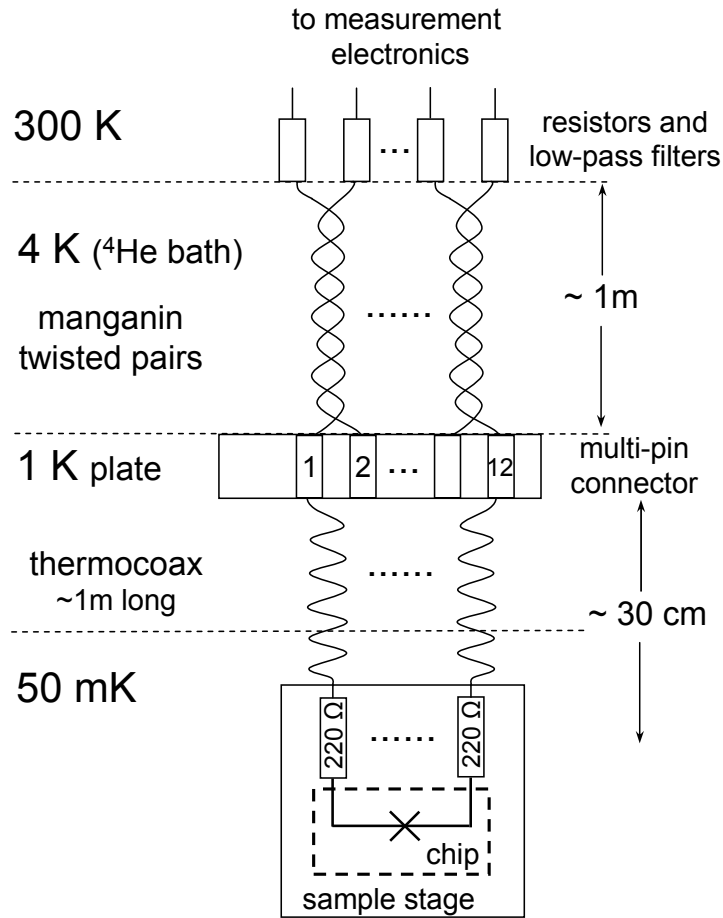
Figure 2.2: Schematics of the cryostat wiring for DC-measurements.

All the pre-amplifiers were powered with batteries. The home made optoisolator, based on commercial optoisolation amplifier Burr-Brown 3650, was used for galvanic decoupling of voltage preamplifiers from digital data reading electronics[3] to avoid digital noise and ground loops. The commercial voltage sources and data acquisition electronics were controlled by Matlab computer software through GPIB IEEE-488 interface bus.

---

[3]data acquisition voltmeter Agilent 34970A.

Chapter 3

Josephson junction as a detector of shot noise

3.1 Shot noise in mesoscopic physics

The electrical fluctuations in a conductor are a consequence of stochastic motion of electrical charges. The intrinsic equilibrium fluctuations of current and voltage in a conductor arise from random thermal motion of its charge carriers at finite temperatures, and they are usually called thermal noise. Another type of electrical fluctuations is shot noise — it appears in a non-equilibrium case, when the conductor is biased with an external current or voltage. Shot noise originates from the finite probability for the discrete electron charges to be transmitted or scattered in the conductor. The effects of shot noise become pronounced in mesoscopic systems, i.e. in conductors with small dimensions, and especially when the conductor is at low temperatures, so that wave properties of the electrons play a dominant role in the charge transport. One of the well-known examples is non-vanishing shot noise in a cold metallic diffusive wire [20] of a length shorter than an electron-phonon relaxation length, the distance on which the electrons thermalize with the atomic lattice of the wire. Moreover, as the wire length is further decreased, the power of shot noise becomes smaller because the number of available electron states, that contribute to the shot noise due to electron-electron scattering, is reduced [21]; the electrons display phase coherent properties at shorter length scales. Thus the studies of shot noise provide information about correlation mechanisms of electron transport in mesoscopic conductors [1, 22, 23].

The noise power, being the second order current correlator, represents the main characteristic of the probability distribution of current fluctuations. However, the distribution of shot noise contains an infinite set of non-vanishing correlators or cumulants of nth-order, $n = 1, 2, ...$ This is in contrast to thermal noise, whose distribution is purely Gaussian — it has only the first and the second order non-zero cumulants. We note that alternatively we can consider the probability $P(N, t)$ that N charge carriers have passed through the conductor in a given time t, since the average current is proportional to the average number of transmitted charges. The recently developed full counting statistics (FCS) of charge transport [2, 3] allows one to calculate the probability distribution $P(N, t)$ and all of its cumulants, thus entirely characterizing the shot noise in

mesoscopic conductors. In case of tunnel junctions, when the electron transport is un-correlated and the transmission probability of the electrons through the tunnel barrier is small, the shot noise at low temperatures is well described by Poisson distribution with all the cumulants equal to the mean value of transmitted charge. From this point of view, a tunnel junction can be used as a reference noise source to study shot noise in different mesoscopic conductors, with sub- or super-Poissonian statistics, (e.g., in carbon nanotubes [24]). Despite of the theoretical advances of FCS, only few experiments on the detection of higher-than-second order fluctuations have been performed, and only in a few mesoscopic systems such as tunnel junctions [4, 25, 26, 27], quantum dots [28, 29], and a quantum point contact [30].

In the first experiment with conventional amplifiers and signal mixers used as de-tectors of the third moment of shot noise [4], the measurement setup was restricted to low impedance samples (50 Ω), resulting in strong feedback effects of electromagnetic environment on the result. In a similar experiment on high impedance samples [25, 30], the circuit corrections were negligibly weak but the bandwidth was limited to low fre-quencies (few tens of MHz). An alternative and perhaps a more natural way to measure noise and FCS of charge in mesoscopic structures is to use another mesoscopic system as an on-chip noise detector. A quantum point contact was successfully used to detect the first five cumulants of electron charge in a quantum dot in the frequency regime of a few tens of kHz [28, 29]. Another choice is to use Josephson junctions as wide bandwidth detectors of noise. They are extremely sensitive to the fluctuations and can be coupled to noise sources with a wide range of impedances. In the experiment with Coulomb blockaded Josephson junction as a detector [26], the influence of high frequency non-Gaussian shot noise on the detector conductance was observed, but mapping the result back to the different cumulants has not been carried out. In this work, we employed a hysteretic Josephson junction as an on-chip threshold detector [31, 32] of non-Gaussian shot noise generated by small tunnel junctions. We studied the shot noise asymmetry by comparing the switching probabilities of the Josephson junction detector for the op-posite directions of the noise current. The detectable bandwidth of fluctuations in our experiment is determined by the plasma frequency of the Josephson junction, which is about 50 GHz.

3.2 Noise characteristics. Full Counting Statistics of charge

We summarize here the noise characteristics and the results of full counting statistics for tunnel junctions, which are used in the analysis of our experiments on the shot noise asymmetry. Let us consider a conductor biased with an external constant voltage V. The instantaneous current $I(t)$ of the conductor fluctuates in time around its average value $\langle I(t) \rangle$ with random variations $\delta I(t) = I(t) - \langle I(t) \rangle$, which can be described by the probability distribution $\rho(I(t))$. Here, we focus our studies on stationary fluctuations, when the average current $\langle I \rangle$ and the nth-order current correlators or central moments

$\langle \delta I(t)^n \rangle = \langle \delta I^n \rangle$ remain constant in time:

$$\langle \delta I^n \rangle = \int_{-\infty}^{\infty} (I - \langle I \rangle)^n \rho(I) dI. \tag{3.1}$$

The low order moments $\langle \delta I^n \rangle$ with $n > 1$ determine the shape of the probability distribution $\rho(I)$: the second moment or the variance $\langle \delta I^2 \rangle$ determines the width of the distribution, the third moment $\langle \delta I^3 \rangle$ — the skewness or the asymmetry of the distribution around the average, and the fourth moment — the kurtosis or the sharpness. In the theory of FCS it is convenient to introduce a characteristic function $\chi(\lambda)$ which is the Fourier transform of $\rho(I)$:

$$\chi(\lambda) = \langle e^{i\lambda I} \rangle = \int_{-\infty}^{\infty} e^{i\lambda I} \rho(I) dI, \tag{3.2}$$

and the cumulants C_n:

$$C_n = (-i)^n \left(\frac{d^n}{d\lambda^n} \ln \chi(\lambda) \right)_{\lambda=0}. \tag{3.3}$$

Once the characteristic function is known for a certain type of the conductor, all the cumulants and thus the probability distribution can be derived, giving the complete characterization of the fluctuations. The cumulants describe how a certain distribution deviates from Gaussian; the lowest four cumulants are related to the central moments as follows: $C_1 = \langle I \rangle$, $C_2 = \langle \delta I^2 \rangle$, $C_3 = \langle \delta I^3 \rangle$, $C_4 = \langle \delta I^4 \rangle - 3\langle \delta I^2 \rangle^2$. Similarly, the cumulants of the number $N(t)$ of transmitted charges in a time t are introduced through the characteristic function of the probability distribution $P(N, t)$. The charge cumulants are related to the current cumulants in the following way:

$$\langle \langle N(t)^n \rangle \rangle = \frac{1}{e^n} \int_0^t \langle I(t_1)...I(t_n) \rangle dt_1...dt_n. \tag{3.4}$$

In the frequency domain the noise is usually characterized by the noise power or the current noise spectral density $S^I(\omega)$. For stationary fluctuations, the noise power at frequency ω is defined through the Fourier transform of the second central moment, which depends only on a time difference $\tau = t_2 - t_1$ between the random events at times t_1 and t_2:

$$S^I(\omega) = \int_{-\infty}^{\infty} \langle \delta I(\tau) \delta I(0) \rangle e^{i\omega\tau} d\tau, \tag{3.5}$$

where we have assumed that noise is invariant in time translation. The time ordering is especially relevant for the third and higher order current correlators and their actual expressions depend on how the noise is detected [33, 34]. The influence of frequency dependent third order correlations on the Josephson junction dynamics is weak, as discussed in Paper II and the appendix of Paper III, and further we consider only non-Gaussian noise in zero-frequency limit. On a long time scale $t \gg \tau$, the cumulants

are proportional to the zero-frequency noise spectral densities:

$$\langle\langle N^2 \rangle\rangle = \frac{t}{e^2} S^I(0), \tag{3.6}$$

$$\langle\langle N^3 \rangle\rangle = \frac{t}{e^3} S_3^I(0). \tag{3.7}$$

Let us discuss the statistics of the transferred charge in zero frequency limit for a coherent conductor (with a length shorter than the electron dephasing length), and the particular case of a tunnel junction. We consider a conductor with transmission coefficients T_j between two normal metal probes (N-c-N), at temperature T, biased with a constant voltage V. The corresponding Fermi distributions of electron energy E on the left and on the right electrodes are $f_L = (1 + e^{(E+eV)/k_B T})^{-1}$ and $f_R = (1 + e^{E/k_B T})^{-1}$. The characteristic function of such a conductor reads [35]

$$\chi(\lambda) = \exp\left[\frac{t}{h}\sum_j \int dE \ln[1 + T_j f_L(1 - f_R)(e^{i\lambda} - 1) + T_j f_R(1 - f_L)(e^{-i\lambda} - 1)]\right], \tag{3.8}$$

where the unity in the argument of the logarithm stands for no transmission, and the second and third terms are the transmission probabilities from left to right and from right to left electrodes in the channel j, correspondingly. The summation is carried out over all the transmission channels of the conductor. In the low temperature limit $k_B T \ll eV$, the characteristic function (3.8) describes the binomial process:

$$\chi(\lambda) = \prod_j [1 + T_j(e^{i\lambda} - 1)]^N \tag{3.9}$$

with the number $N = eVt/h$ of attempts for the electron in channel j to be transmitted through the scattering region with success probability T_j in a time t. Expanding Eq. (3.8) in charge cumulants we find that the cumulants are proportional to the average number of transmitted charges $\langle N \rangle$:

$$\langle\langle N \rangle\rangle = \langle N \rangle \sum_j T_j, \tag{3.10}$$

$$\langle\langle N^2 \rangle\rangle = \langle N \rangle \sum_j T_j(1 - T_j), \tag{3.11}$$

$$\langle\langle N^3 \rangle\rangle = \langle N \rangle \sum_j T_j(1 - T_j)(1 - 2T_j). \tag{3.12}$$

In the case of a tunnel junction (NIN), when all the transmission probabilities are small, $T_j \ll 1$, the characteristic function (3.8) reduces to:

$$\chi(\lambda) \approx \exp[-\frac{Vt}{eR_T}\left(\coth\left(\frac{eV}{2k_B T}\right)(1 - \cos\lambda) + i\sin\lambda\right)], \tag{3.13}$$

where $R_T = \left(\frac{e^2}{h}\sum_j T_j\right)^{-1}$ is the tunneling resistance of the junction. The charge cumulants are thus given by:

$$\langle\langle N(t)^n \rangle\rangle = \begin{cases} \frac{\langle I \rangle t}{e} \coth(\frac{eV}{2k_B T}), & \text{if } n \text{ is even,} \\ \frac{\langle I \rangle t}{e}, & \text{if } n \text{ is odd} \end{cases}$$

Thus, the zero-frequency noise power for the tunnel junction with the average current $\bar{I} = \langle I \rangle = V/R_T$ is:

$$S^I(0) = e\bar{I} \coth(\frac{eV}{2k_B T}). \tag{3.14}$$

In the limit $k_B T \ll eV$, the binomial distribution $P(N, t)$ of the tunnel junction reduces to Poissonian:

$$P(N, t) = \frac{\langle N \rangle^N}{N!} e^{-\langle N \rangle}, \tag{3.15}$$

with all the cumulants equal to the mean value $\langle N \rangle$ of charge. This is the case of pure shot noise:

$$S^I(0) = e\bar{I}, \tag{3.16}$$

$$S_3^I(0) = e^2 \bar{I}. \tag{3.17}$$

For a N-c-N conductor the shot noise is reduced with respect to Poissonian by Fano factors (F_2 and F_3):

$$S^I(0) = F_2 e\bar{I}, \quad F_2 = \frac{\sum_j T_j(1 - T_j)}{\sum_j T_j} \tag{3.18}$$

$$S_3^I(0) = F_3 e^2 \bar{I}, \quad F_3 = \frac{\sum_j T_j(1 - T_j)(1 - 2T_j)}{\sum_j T_j} \tag{3.19}$$

The Fano factors give information about the correlation of electron transport in a conductor as compared to that of the tunnel junction, for which all the Fano factors equal unity, $F_2 = F_3 = ... = F_n = 1$. Thus a tunnel junction can be used as a reference noise source in studies of shot noise of other conductors [24].

The comparison of Poisson and Gaussian distributions is shown in Fig. 3.1. For the Poisson distribution, the positive fluctuations (with the same sign as the average current) occur with larger probability than the negative fluctuations, and thus the shot noise distribution is asymmetric with respect to the average current. Such an asymmetry arises due to the odd moments of the Poisson distribution. For large currents $I \gg e\omega_p$ as in our experiment, the asymmetry is exponentially weak (due to the central limit theorem), and it is pronounced only on the tails of the Poissonian distribution (Fig. 3.1b). To detect such a weak asymmetry, we use a Josephson junction threshold detector. It has exponential sensitivity to the current fluctuations in a very wide frequency bandwidth determined by the plasma frequency $\omega_p/2\pi$ of the junction, which is about 50 GHz in our case. Throughout we ignore the supposedly negligible contributions of the fourth and higher order fluctuations. In the experiments we describe the shot noise with a white, i.e. frequency independent spectrum up to the relevant frequency scale $\omega_p/2\pi$.
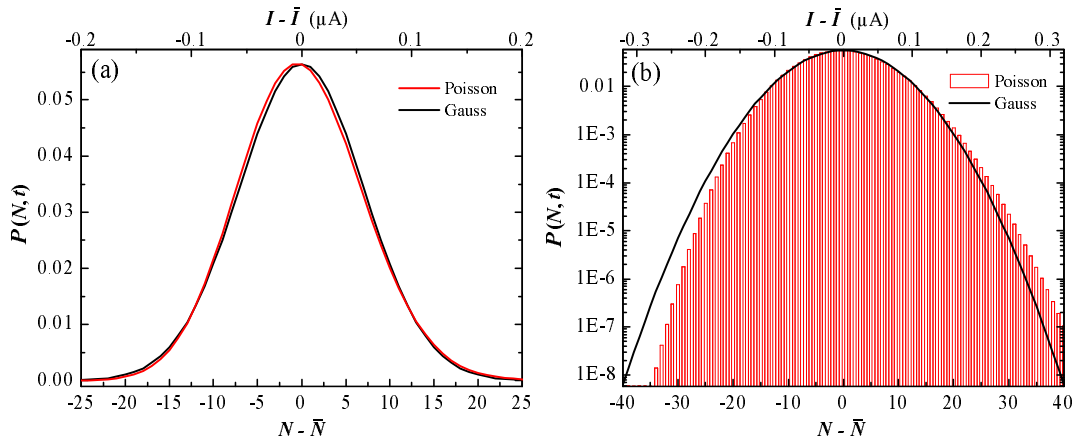
Figure 3.1: Poisson distribution $P(N, t)$ of shot noise in the tunnel junction is compared to the Gaussian distribution with the same variance. The distributions are calculated with the average number of charges $\bar{N} = 50$ (which corresponds to the average current $\bar{I} = 0.4$ μA), transmitted in a time $2\pi/\omega_{\mathrm{p}}$ ($\omega_{\mathrm{p}}/2\pi = 50$ GHz), which is the typical response time of the Josephson junction detector. The shot noise asymmetry is clearly visible only on the logarithm scale in panel (b), showing that the effects of non-Gaussian noise are exponentially weak.

3.3 Influence of noise on Josephson junction dynamics

A Josephson junction was recently proposed [31, 32] as a threshold detector of full counting statistics of electrical current. Indeed, a Josephson junction is a natural current threshold detector, which ideally would instantaneously switch from a superconducting zero-voltage state to the normal finite-voltage state (escape out of a metastable state) each time when the current $I = I_0 + \delta I$ through it exceeds the critical current I_c. Here, I_0 is a constant bias current, and δI is an external fluctuating current from a nearby mesoscopic conductor to be investigated. The switching probability $P_{\mathrm{sw}}^0(I_0)$ of such an ideal detector would be straightforwardly related to the distribution of current fluctuations $\rho(\delta I)$, $P_{\mathrm{sw}}^0(I_0) = \int_{I_c-I_0}^{\infty} \rho(\delta I)d(\delta I)$. In a real situation, we have to take into account the influence of thermal and quantum fluctuations on the escape. Also, the Josephson junction has a finite response time, determined by the plasma frequency ω_{p}, since its resonant activation represents a sharp cut-off around ω_{p} [36]. Therefore the escape is not affected by the fluctuations on a time scale faster than $\tau = 2\pi/\omega_{\mathrm{p}}$, but it is determined by the noise at plasma and sub-plasma frequencies. In the experiment, we probe the escape with current pulses I_0 of duration $\Delta t \gg \tau$. The switching probability measured in the experiment depends on the fluctuating current through the escape rate $\Gamma(I_0 + \delta I)$, $P_{\mathrm{sw}} = 1 - e^{-\Gamma(I_0+\delta I)\Delta t}$. Below, we consider the escape dynamics of the Josephson junction and the influence of noise on the escape rates.

3.3.1   Escape dynamics in thermal activation regime

We first discuss the escape process in the absence of shot noise. The phase dynamics of a Josephson junction can be well described by the Resistively and Capacitively Shunted Junction model (Fig. 3.2). The equivalent circuit represents an ideal junction with a supercurrent $I_c \sin \varphi$ in a parallel combination with a capacitance C and a frequency-dependent admittance $Y(\omega) = 1/Z(\omega)$, which is an inverse impedance $Z(\omega)$ of the surrounding electromagnetic circuit. The junction is biased with the current $I(t) = I_0 + \delta I(t)$, where the fluctuating current component $\delta I(t)$ arises due to the equilibrium thermal noise generated in the admittance $Y(\omega)$. In the simplest case of a frequency-independent ohmic environment $Y(\omega) = 1/R$, when the impedance is a pure resistor $Z(\omega) = R$, $\delta I(t)$ represents a white Gaussian noise with the variance $\langle \delta I(t) \delta I(t') \rangle = 2k_B T \delta(t - t')/R$. In the classical regime of high temperatures $k_B T \gg \hbar \omega_{\mathrm{p}}$, the phase
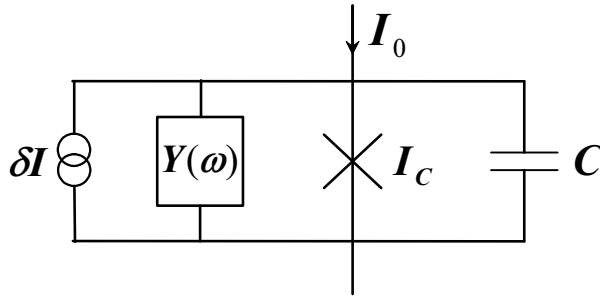
Figure 3.2: Resistively and Capacitively Shunted model of a Josephson junction.

dynamics is described by the equation

$$\frac{\hbar}{2e}(I_0 + \delta I(t)) = \partial_\varphi U(\varphi) + \frac{1}{R}\left(\frac{\hbar}{2e}\right)^2 \dot{\varphi} + C\left(\frac{\hbar}{2e}\right)^2 \ddot{\varphi}. \qquad (3.20)$$

where the dot denotes time derivative. The equation (3.20) can be interpreted as an equation of motion of a phase particle of a mass $m = (\hbar/2e)^2 C$ with kinetic energy $\dfrac{\hbar^2 \ddot{\varphi}}{8E_C}$ in a tilted cosine washboard potential $U(\varphi) = -E_J(\dfrac{I_0}{I_c}\varphi + \cos\varphi)$, affected by the damping force $\left(\dfrac{\hbar}{2e}\right)^2 \dfrac{\dot{\varphi}}{R}$ and the stochastic force $\dfrac{\hbar}{2e}\delta I(t)$. Here, $E_J = \dfrac{\hbar I_c}{2e}$ is the Josephson energy and $E_C = \dfrac{e^2}{2C}$ is the charging energy of the junction. At low enough currents $I \ll I_c$, the particle stays at one of the minima of the potential, oscillating with the plasma frequency $\omega_{\mathrm{p}} = \sqrt{8E_J E_C \varphi_0}/\hbar$, where $\varphi_0 = \sqrt{1 - (I_0/I_c)^2}$ is a renormalization of the oscillating frequency due to the bias-dependent tilt of the potential. As the bias current is increased towards the critical current, the height of the potential ΔU is reduced, and the particle can escape out of the well over the barrier due to thermal fluctuations. The

decay rate of the metastable state in this thermal activation (TA) regime is proportional to the frequency of escape attempts $\omega_{\mathrm{p}}/2\pi$ and the Boltzmann activation factor:

$$\Gamma_{\mathrm{TA}}(I) \simeq \frac{\omega_{\mathrm{p}}}{2\pi} e^{-\frac{\Delta U(I)}{k_B T}}, \qquad (3.21)$$

where the barrier $U(\varphi)$ is well approximated by the cubic parabola at currents $I_0/I_c \to 1$, with the height $\Delta U(I_0) \simeq (4\sqrt{2}/3)E_J(1-I_0/I_c)^{3/2}$. The damping of the phase motion at plasma frequency is given by the quality factor $Q = \omega_{\mathrm{p}}\mathrm{Re}[\mathrm{Z}(\omega_{\mathrm{p}})]\mathrm{C}$. The value of $Q > 1$ corresponds to underdamped junctions. Then the particle, once escaped, rolls down over many potential minima before being retrapped. $Q < 1$ corresponds to overdamped junctions, when the particle gets retrapped in the very next minimum when escaped. In our experiments, we use underdamped Josephson junctions as noise detectors. The transition from the normal state back to the superconducting state in underdamped junctions occurs when the biasing current becomes lower than the retrapping current $I_r \simeq 4I_c/\pi Q_r$, so that the dissipated energy of the rolling particle exceeds the energy difference between two adjacent local minima of the Josephson tilted potential. Here, Q_r is the quality factor at low frequencies, determined by the electromagnetic environment of the junction, generally different from $Q(\omega_{\mathrm{p}})$ at plasma frequency.

3.3.2 Underdamped phase diffusion

In the superconducting state the voltage across the junction is not necessarily zero. The 2π-slips of the phase lead to a small average voltage across the junction. When the temperature becomes comparable with the barrier height, although remaining lower $k_B T \lesssim E_J$, there is a finite probability that, upon escape from the well, the oscillating particle is retrapped in the next well instead of running down the potential, if the dissipation is strong ($Q \gtrsim 1$). The phase then moves diffusively from one well to another. This is the case of underdamped phase diffusion [37, 38, 39]. The maximum possible phase diffusion current is given by $I_d = 4I_c/\pi Q(\omega_{\mathrm{p}})$. For bias currents $I_0 < I_d$ there is a non-zero probability that the phase relocalizes after the escape. The rate of the phase diffusion events can be estimated from the finite voltage V_d in the supercurrent branch as $2eV_d/h$.

3.3.3 Escape in the macroscopic quantum tunneling regime

In the quantum limit which is achieved at low temperatures $\hbar\omega_{\mathrm{p}} \gg k_B T$ as in our experiment, the behavior of the junction is described by the hamiltonian with charge $q = CV$ and phase φ being the quantum conjugated variables, $[\hat{q}, \hat{\varphi}] = 2ei$:

$$\mathcal{H} = \frac{\hat{q}^2}{2C} - E_J \cos\hat{\varphi} - \frac{\hbar}{2e}I\hat{\varphi}. \qquad (3.22)$$

The junction with $E_J \gg E_c$ can be considered as a quantum system with the number $\sim \Delta U(I_0)/\hbar\omega_{\mathrm{p}}$ of discrete energy levels within the metastable potential well. The distance

between adjacent levels is determined approximately by the plasma frequency ω_{p}. Due to quantum fluctuations, the phase can escape from the well by tunneling through the barrier. In such macroscopic quantum tunneling (MQT) regime the escape rate (in the absence of shot noise) is given by

$$\Gamma_{\mathrm{MQT}} = A(I)e^{-B(I)} \tag{3.23}$$

with

$$A(I) = \frac{\omega_{\mathrm{p}}}{2\pi} 12\sqrt{6\pi}\sqrt{\frac{\Delta U}{\hbar\omega_{\mathrm{p}}}} \tag{3.24}$$

and

$$B(I) = \frac{36}{5}\frac{\Delta U}{\hbar\omega_{\mathrm{p}}}. \tag{3.25}$$

This follows from the treatment of tunneling out of a cubic potential in the semiclassical limit $E_J \gg E_C$ with low damping. Also, in the lowest order approximation the well can be considered as parabolic, with the energy levels of a harmonic oscillator: $E_n = \hbar\omega_{\mathrm{p}}(n + 1/2)$. The crossover between TA and MQT regimes occurs at temperature $T_{cr} \simeq \hbar\omega_{\mathrm{p}}/2\pi k_B$.
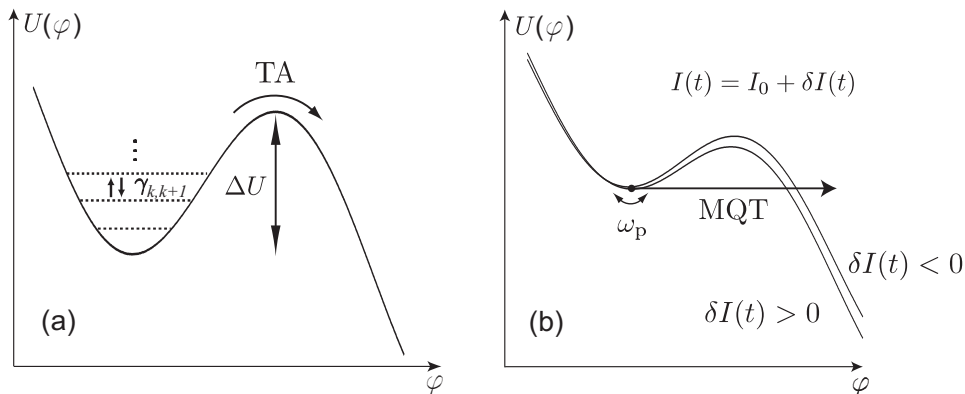
Figure 3.3: (a) Thermally activated escape. The transitions between energy levels in the well are induced by shot noise. (b) Macroscopic quantum tunneling. The effect of fluctuations at sub-plasma frequencies is to slowly vary the Josephson potential around its average value.

3.3.4   Influence of Gaussian noise on the escape

The noise strongly affects the phase dynamics of the Josephson junction and modifies the escape rate. We first discuss the influence of the second order fluctuations on the escape in the MQT regime. The effect of noise is to induce transitions between different energy levels in the potential well [40]. The result of the Fermi Golden rule calculations

is that the transition rate $\gamma_{m,n}$ between the m:th and the n:th level is proportional to the noise spectral density $S_{\text{tot}}^I(\omega)$ at the level spacing frequency $\omega_{m,n}$:

$$\gamma_{m,n} = \frac{1}{\hbar^2}|M_{m,n}|^2 S_{\text{tot}}^I(\omega_{m,n}), \tag{3.26}$$

where the matrix element $M_{m,n} \equiv \hbar\hat{\varphi}/2e$ determines the transition probability between the levels. Relaxation (excitation) rate is determined by the noise spectral density at positive (negative) frequencies. Due to nearly harmonic shape of the well, the transitions between neighboring levels are dominating in the well dynamics. The level spacing is then determined by the plasma frequency ω_{p}, and the matrix elements between the adjacent levels k and $k+1$ can be approximated by $|M_{k,k+1}|^2 \simeq k/(2\hbar\omega_{\text{p}}C)$. The noise spectrum $S_{\text{tot}}^I = \int_{-\infty}^{\infty}\langle\delta I(t)\delta I(0)\rangle\exp(i\omega t)d\omega$ has two contributions, $S_{\text{tot}}^I = S_{\text{env}}^I + S^I$, one due to equilibrium environment S_{env}^I, and the other due to the shot noise S^I.

The spectrum of equilibrium noise is related to the admittance of the junction circuit $Y(\omega)$ via the fluctuation-dissipation theorem:

$$S_{\text{env}}^I(\omega) = \hbar\omega\text{Re}[Y(\omega)]\left[\coth\left(\frac{\hbar\omega}{2k_BT}\right) + 1\right]. \tag{3.27}$$

At low bath temperatures $k_BT \ll \hbar\omega_{\text{p}}$ as in our case, the excitation due to equilibrium environment noise is strongly suppressed, $S_{\text{env}}^I(\omega < 0) \to 0$, and the relaxation occurs due to quantum fluctuations of the environment, $S_{\text{env}}^I(\omega > 0) \to 2\hbar\omega\text{Re}Y(\omega)$.

The shot noise (from the noise source with a current $\bar{I}_{\text{N}}$ as in the experiment) with a spectrum

$$S^I(\omega) = eF_2^{\text{eff}}\bar{I}_{\text{N}}, \tag{3.28}$$

induces both excitations and relaxations in the well. Here $F_2^{\text{eff}} = F_2 G(\omega)G(-\omega)$ is the effective Fano factor. The frequency-dependent factor $G(\omega)$ characterizes the circuit impedance between the noise source and the detector junction, by relating the fluctuating current δI through the detector to the fluctuations δI_{N} as $\delta I(\omega) = G(\omega)\delta I_{\text{N}}$. We would have $F_2^{\text{eff}} = 1$ in case of an ideal Poisson noise source and if all the shot noise would run through the detector junction.

The influence of noise on the level dynamics can be taken into account by requiring that excitation and relaxation rates are described with pure equilibrium fluctuations at an effective noise temperature $T^\star$. The effective temperature can be then expressed as [40]:

$$k_BT^\star \simeq \hbar\omega_{\text{p}} \ / \ 2\text{arcoth}[1 + \frac{F_2^{\text{eff}}e|\bar{I}_{\text{N}}|Q}{\hbar\omega_{\text{p}}^2C}], \tag{3.29}$$

and the escape rate is given by

$$\Gamma \simeq \frac{\omega_{\text{p}}}{2\pi}e^{-\frac{\Delta U}{k_BT^\star}}. \tag{3.30}$$

The effective temperature model is valid at high noise temperatures $T^\star > T_{cr}$, when the thermal activation due to equilibrium bath fluctuations is weak. In the limit of large noise

currents $|\bar{I}_N| \gg \hbar\omega_p^2 C/(eQF_2^{\text{eff}})$, the effective temperature can be further approximated by

$$k_B T^\star \simeq \frac{QF_2^{\text{eff}} e|\bar{I}_N|}{2\omega_p C} = \frac{e|\bar{I}_N| R F_2^{\text{eff}}}{2}, \tag{3.31}$$

where $R = Q/\omega_p C$ is the effective real part of the circuit impedance.

Thus the influence of the second moment of shot noise on the escape is taken into account through the resonant transitions at plasma frequency ω_p. This leads to the thermally activated escape at the effective noise temperature $T^\star$ (3.29).

3.3.5 Influence of non-Gaussian noise on the escape

The influence of the third order fluctuations on the transition rates can be taken into account via higher order perturbation corrections to the Fermi golden rule result (3.26), and also including the anharmonicity of the cubic potential. However, the effect on the resonant transitions due to the third order fluctuations is weak and vanishes in a strictly harmonic potential. Also in the case of anharmonic potential, the corrections vanish for the frequency independent third order spectral density [41, 34],[Paper II]. Therefore we consider in what follows the effect of non-Gaussian fluctuations at sub-plasma frequencies. The effect of such fluctuations is to slowly vary the tilt of the washboard potential around its average value. We can then describe the escape rate (3.23) by averaging over the distribution of slow fluctuations as follows. The escape rate up to the first order in the exponent is given by:

$$\Gamma(I_0 + \delta I) \simeq \Gamma(I_0) \exp\left[-\left(\frac{\partial B}{\partial I}\right)_{I=I_0} \delta I\right], \tag{3.32}$$

where the effect of the second moment of shot noise on the escape rate is accounted for by the dependence of $B = \Delta U/k_B T^\star$ on the effective temperature. Neglecting the weak current dependence of the prefactor $A(I)$ (3.24), we can identify the averaged escape rate $\langle\Gamma(I)\rangle$ over sub-plasma fluctuations with the moment generating characteristic function (3.2):

$$\langle\Gamma(I)\rangle = \Gamma(I_0)\langle e^{\lambda\delta I}\rangle = \Gamma(I_0)\int_{-\infty}^{\infty} \rho(\delta I)d(\delta I)e^{\lambda\delta I}, \quad \lambda \equiv -\left(\frac{\partial B}{\partial I}\right)_{I=I_0}. \tag{3.33}$$

Expanding the exponent $\langle e^{\lambda\delta I}\rangle$ up to the third cumulant of δI, we get

$$\langle\Gamma\rangle \simeq \Gamma(I_0) \exp\left[\frac{1}{2}\left(\frac{\partial B}{\partial I}\right)^2 \langle\delta I^2\rangle - \frac{1}{6}\left(\frac{\partial B}{\partial I}\right)^3 \langle\delta I^3\rangle\right]. \tag{3.34}$$

Taking into account that the odd moments of shot noise change the sign when changing the sign of the fluctuations (the polarity of the noise current in the experiment), the asymmetry

$$\frac{\Delta\Gamma}{\Gamma_{\text{ave}}} \equiv \frac{\langle\Gamma^+\rangle - \langle\Gamma^-\rangle}{\frac{1}{2}(\langle\Gamma^+\rangle + \langle\Gamma^-\rangle)} \tag{3.35}$$

between escape rates $\langle \Gamma^{\pm} \rangle$ at different polarities of either pulse or noise currents can then be written as:

$$\frac{\Delta\Gamma}{\Gamma_{\text{ave}}} \simeq -\frac{1}{3} \left(\frac{\partial B}{\partial I} \right)_{I=I_0} \langle \delta I^3 \rangle, \tag{3.36}$$

or via an effective temperature

$$\frac{\Delta\Gamma}{\Gamma_{\text{ave}}} \simeq \frac{16\sqrt{2}}{3} \left(\frac{\hbar}{2e} \right)^3 (1 - I_0/I_c)^{3/2} \frac{\langle \delta I^3 \rangle}{(k_B T^\star)^3}. \tag{3.37}$$

Here, $\langle \delta I^3 \rangle = (\frac{\Delta\omega}{2\pi})^2 S_3(0)$, where $\Delta\omega \sim \omega_{\text{p}}$ is the bandwidth of the fluctuations, and $S_3^I = e^2 \bar{I} F_3$ is the low frequency limit of the third order spectral density with Fano factor F_3. The rate asymmetry (3.37) can be measured directly in the experiment allowing to determine the intensity and the sign of the third order fluctuations.

3.4 Experimental setup and results

The picture of the studied sample with the employed measurement circuit is shown in Fig. 3.4. The Josephson junction detector is an Al-AlOx-Al SIS junction of an area

Figure 3.4: Measurement scheme with an optical image of the sample. The currents $\pm I_0$ and $\pm I_N$ are injected into the structure through large (200 kΩ and 5 MΩ) resistors at room temperature. The current amplifier with low input impedance connected to the other side of the JJ detector verifies the DC-current balance. The voltage V across the JJ detector is measured by a high impedance (> 1 GΩ) voltage amplifier. The sketch below depicts details of the structure.

of $\simeq 2$ μm^2. It is connected to the shot noise source via a superconducting line. The noise source is another SIS or NIS tunnel junction with an area of $\simeq 0.2$ μm^2. It is biased with the DC current $\pm I_N \gg \Delta/(eR_N)$ above the superconducting gap Δ into the shot noise regime (R_N is a tunnel resistance of the noise junction). Simultaneously, a balancing current $\mp \bar{I}_N$ of the opposite polarity is applied so that no DC component $\bar{I}_N$ of

the noise current flows through the detector, and only fluctuations are admitted across it. The balance of the DC-currents through the detector is verified with a low input impedance current amplifier within the accuracy of < 1 nA. To suppress the leakage of shot noise into the bias lines, narrow (2 μm) and few millimeters long superconducting inductive leads are used on the chip for the current injection. The superconducting line between the detector and the noise source is 12 μm wide to lower the inductance and obtain better noise coupling. The large bonding pad with an area ~ 1 mm^2 close to the detector junction plays a role of a capacitor of ~ 1 pF to shunt the noise. The distance between the detector and the noise source is about 100 μm to avoid overheating of the detector due to the Joule heating from the noise source.

We report results on two samples which we denote as NIS and SIS, corresponding to the actual noise source junction in the sample. The on-chip design of sample SIS was slightly different from that of sample NIS — the superconducting line between the detector and the noise source was narrower (2 μm), and the inductive lines were shorter (~ 1 mm). The parameters of the samples are given in the table I. The shot noise

Table 3.1: Parameters of the samples.

Sample	detector			noise junction
	I_c (μA)	C (fF)	$\frac{\omega_{p0}}{2\pi} = \frac{1}{2\pi}\sqrt{\frac{2eI_c}{\hbar C}}$ (GHz)	R_N (kΩ)
SIS	2.51	80	49	1.9
NIS	2.88	80	53	15.4

measurements were carried out at the base temperature of 30 mK. The two samples showed similar behavior, and below we refer to the data on sample NIS unless otherwise specified. A rough idea of the shot noise influence on the Josephson junction detector can be obtained from the detector IV characteristics shown in Fig. 3.5a. With an increase of the average noise current $\bar{I}_N$, the switching threshold current of the detector gets suppressed. In the supercurrent branch, the weak slope of the IV curve is such that the voltage V_d is below 0.2 μV up to the switching current. This gives an estimate for the rate of the phase diffusion events from one well to another — $2eV_d/h < 100$ MHz. Also, the gap voltage is constant in the wide range of noise current $\bar{I}_N$ up to 5 μA. This indicates that there is no excess overheating of the bath and that the escape dynamics can be described in terms of the effective noise temperature T_{eff}.

To study the influence of the shot noise on the escape dynamics in more detail, the current pulses of duration $\Delta t = 100$ μs - 3 ms and of amplitude I_0 are applied at different values of noise currents $\bar{I}_N$, so that the noise is imposed on top of the pulse, and the escape probability $P(I_0)$ is obtained as a fraction of the current pulses which led to voltage pulses across the detector junction. Typically 10^3 - 10^4 pulses at each current amplitude I_0 are applied to obtain good statistics for the escape probability. The time delay between the pulses was 1 ms or longer to allow the detector junction to be retrapped back into the superconducting state after the escape before the next
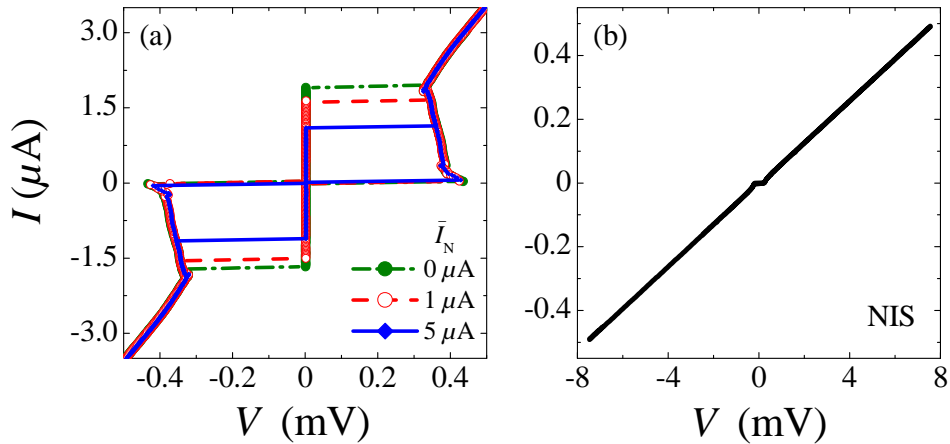
Figure 3.5: (a) Current-voltage characteristics of the detector at different noise currents $I_N = 0, 1, 5$ μA. (b) An $I - V$ characteristic of NIS noise source.

pulse. The average escape rate $\langle \Gamma(I_0) \rangle$ can be deduced from the escape probability as $\langle \Gamma(I_0) \rangle = -\ln(1 - P(I_0))/\Delta t$. The escape histogram $P(I_0)$ is typically characterized by the current threshold $I_{0.5} = I_0(P = 0.5)$, and the width $\Delta I = I_0(P = 0.9) - I_0(P = 0.1)$.

The measured escape histogram $P(I_0)$ of the detector junction as a function of the current pulse amplitude I_0 in the MQT regime (with no noise current applied, $\bar{I}_N = 0$) is shown in Fig. 3.6. The given values of critical current I_c and capacitance C for the detector are obtained from the MQT fit to the escape histogram in Fig. 3.6. The plasma frequency of the detector at zero bias current $I_0 = 0$ is then determined as $\omega_{p0} = \sqrt{\frac{2eI_c}{\hbar C}}$. It gives the relevant detectable bandwidth of fluctuations up to $\Delta\omega/2\pi \sim 50$ GHz.

The increase of the average noise current $|\bar{I}_N|$ and hence of the noise power leads to the enhancement of the escape rate, and consequently the threshold current gets suppressed resulting in a significant shift of a histogram towards lower pulse amplitudes I_0. This is the dominating effect on the escape due to the second moment of the shot noise [40]. To study the influence of the third moment on the escape, the switching probability is measured with four different combinations of current polarities: I^{++}, I^{--}, I^{+-}, and I^{-+}. Here the first superscript refers to the sign of the pulse I_0, and the second to that of the noise current $\bar{I}_N$. One pair of the escape characteristics, $P(+I_0, +\bar{I}_N)$ and $P(-I_0, -\bar{I}_N)$, should give mutually identical results, since the pulse current and fluctuations are of the same polarity. Similarly, the second pair, $P(+I_0, -\bar{I}_N)$ and $P(-I_0, +\bar{I}_N)$, should also lead to an identical result, which is different from that of the first pair due to the presence of odd moments. Indeed, for positive skewness of shot noise distribution, the threshold current for the pair of histograms $P(+I_0, +\bar{I}_N)$, $P(-I_0, -\bar{I}_N)$ is expected to be lower than that for the other pair. In the experiment, we detect the small shift of the threshold current between the two pairs of histograms at each value of $\bar{I}_N$, $I^+ - I^- = \frac{1}{2}[(I^{+-} + I^{-+}) - (I^{++} + I^{--})]$. On this short current interval $I^+ - I^-$, we can make
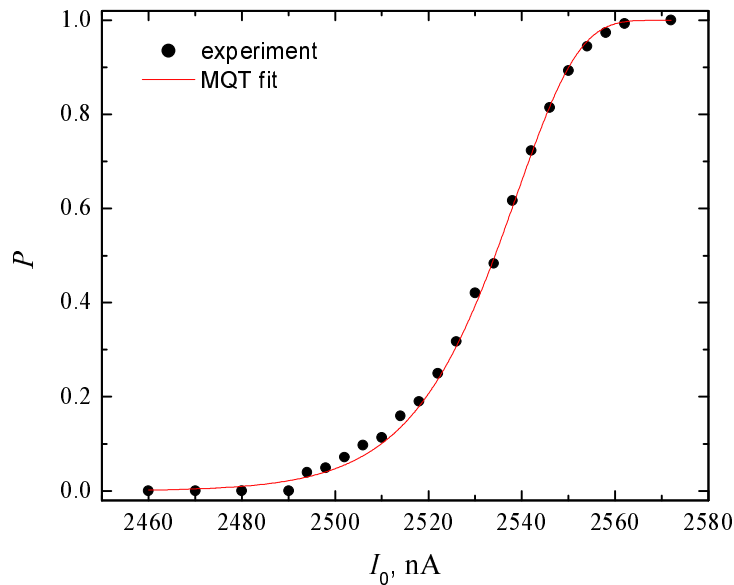
Figure 3.6: The measured escape histogram of the detector of sample NIS with pulse length $\Delta t = 480$ μs. The fit to the data using MQT escape rate (Eq. 3.23) is shown by the solid line.

a linear approximation of $P(I_0)$ on I_0 and express the current shift through the rate asymmetry (3.35) $\Delta\Gamma/\Gamma_{\text{ave}} \equiv \frac{\langle\Gamma^+\rangle - \langle\Gamma^-\rangle}{0.5(\langle\Gamma^+\rangle + \langle\Gamma^-\rangle)}$:

$$I^+ - I^- \simeq (1-P)\ln(1-P)\left(\frac{\partial P}{\partial I_0}\right)^{-1}\left(\frac{\Delta\Gamma}{\Gamma_{\text{ave}}}\right). \tag{3.38}$$

The measured results on the influence of shot noise on the escape histograms for sample NIS are shown on Fig. 3.7. Suppression of the mean threshold current with increasing $\bar{I}_N$ and change in the width is evident from the histograms. Furthermore, the pair of histograms P^{++} and P^{--} lie on top of each other and similarly data P^{+-} lies on top of P^{-+}. The switching threshold currents for the latter two polarity combinations lie at higher values of I_0 than for the former one. This experimental result is consistent with what we expect due to positive skewness of the current distribution.

Before analyzing the shot noise asymmetry, let us first discuss the effect of the second moment of shot noise on the escape. The width of the histograms, plotted in Fig. 3.8b, has a non-monotonic behavior. We attribute the maximum of the width at the noise current $\bar{I}_N = 2.6$ μA to the crossover from the escape dynamics to the underdamped phase diffusion [37, 38, 39], now induced by the effective temperature. This is typical behavior of the width of the escape histogram as a function of temperature when the phase diffusion sets in [16, 37]. From the value $I_{0.5} \simeq 0.52I_c$ of the threshold current
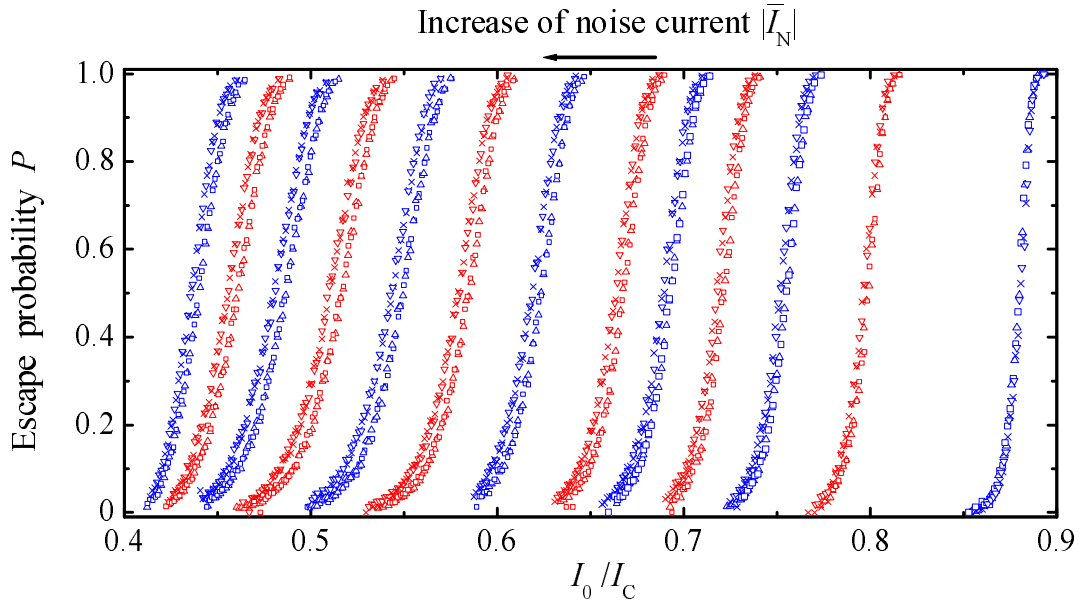
Figure 3.7: Measured escape histograms for different combinations of the pulse and the noise current polarities [$I^{+-}(\triangle)$ and $I^{-+}(\square)$, $I^{++}(\triangledown)$ and $I^{--}(\times)$] at different values of the average noise current $\bar{I}_N = 0...3.8\ \mu A$.

for histograms at $\bar{I}_N = 2.6\ \mu A$, we obtain the quality factor $Q(\omega_p) = 4I_c/\pi I_{0.5} = 2.5$ at plasma frequency.

The suppression of the threshold current due to the increase of the noise power can be described by the model of the resonant activation at the effective temperature (3.29). The effective temperature, obtained from the histograms positions at $P = 0.1$; 0.5; and 0.9, is plotted in Fig. 3.8a. The result of the model (3.29) with the parameters $F_2^{\text{eff}} = 1$ and $Q = 2.5$ for $P = 0.5$ is shown by the solid line, and it is in good agreement with the data up to $|\bar{I}_N| \simeq 2.6\ \mu A$. At higher noise currents $|\bar{I}_N| > 2.6\ \mu A$ the effective temperature is not single-valued and deviates from the theoretical result particularly for $P = 0.1$ due to the onset of phase diffusion. This is quite natural because here the bias current is lowest which favors phase diffusion. Also, the result for the histogram width from the effective temperature model in Fig. 3.8b lies above the data and does not predict the non-monotonic behavior of the histogram width. For more accurate analysis, both the escape and retrapping processes have to be taken into account [42]. For Sample SIS the measurements yielded a similar result, with $F_2^{\text{eff}} = 1$ and $Q = 2.5$.

Let us focus now on the effects of non-Gaussian noise on the escape which is the main result of this work. The shot noise asymmetry deduced from the escape histograms (Fig. 3.7) for samples NIS and SIS is shown in Fig. 3.9 in a from of $(I^+ - I^-)/I_c$ for $P = 0.5$. The open circles refer to the vanishing signal when the current $\bar{I}_N$ is injected through the supercondcuting line without the noise source. Also, in sample SIS the signal vanishes when the noise source is in the superconducting state at $\bar{I}_N <$
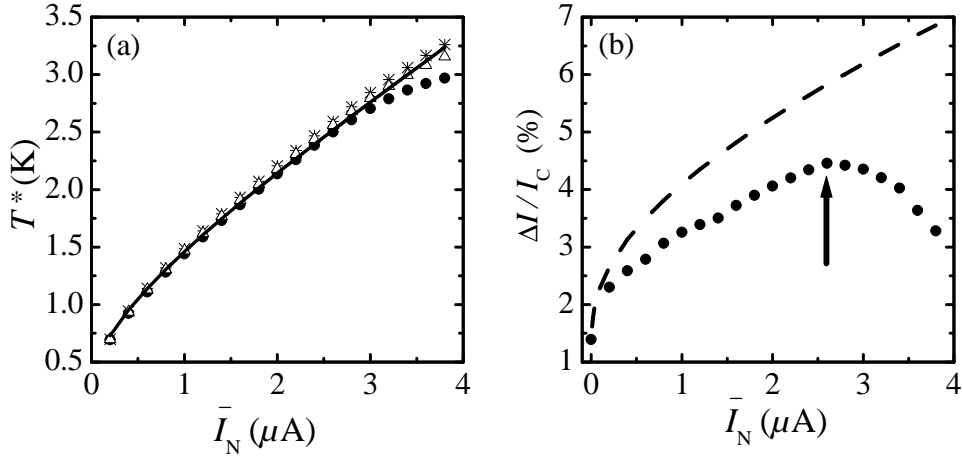
Figure 3.8: Results related to the second moment of shot noise. (a) Effective temperature $T^\star$ extracted from measured escape histograms using Eq. (3.30) for $P = 0.1$ ($\bullet$), 0.5 ($\triangle$), and 0.9 ($\ast$). The solid line is obtained using Eq. (3.29) with $F_2^{\text{eff}} = 1$ and $Q = 2.5$ determined from the bias current at which the underdamped phase diffusion sets in. This is shown by the arrow in (b), where the width of the histogram is plotted against $\bar{I}_\text{N}$. The dashed line is from the effective temperature model, ignoring phase diffusion.
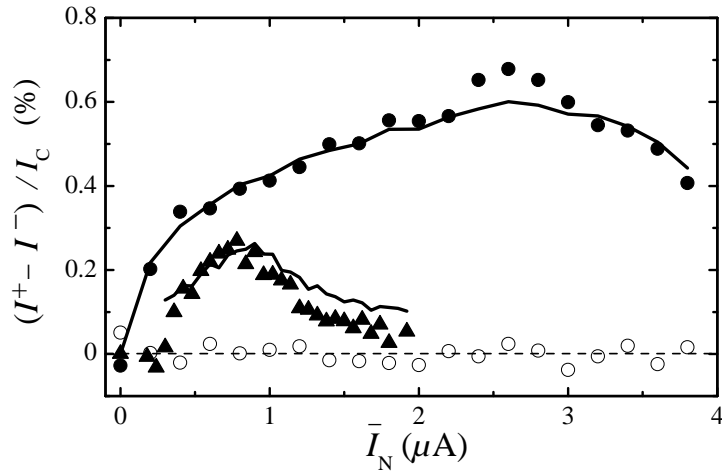
Figure 3.9: The measured shot noise asymmetry for sample NIS (filled dots) and sample SIS (triangles). The open circles are the results of reference measurements. The solid lines are the result of the theoretical model for Samples NIS and SIS. At currents $\bar{I}_\text{N} \leq 0.2$ μA the noise source of Sample SIS is in superconducting state, and the signal due to shot noise vanishes.

0.2 μA. This verifies the good balance of the injected DC-currents. As expected, the measured asymmetry corresponds to the positive third moment of shot noise $\langle \delta I^3 \rangle = e^2 F_3 \bar{I}_\text{N} \left(\frac{\Delta\omega}{2\pi} \right)^2$. The solid lines in Fig. 3.9 are the results of the model of slow non-Gaussian fluctuations at sub-plasma frequencies. The lines are constructed using Eqs. (3.37) and (3.38), with parameters $(\partial P/\partial I)$ and $T^\star$ extracted from the experiment. Due

to the experimentally determined derivatives $(\partial P/\partial I_0)_{I_{0.5}}$ from the linear interpolation of the histograms around $P = 0.5$, the fit lines are not smooth. The only fit parameter in the model is then the bandwidth of the third order fluctuations $\Delta\omega$ (assuming Fano factor $F_3 = 1$). For sample NIS, we have set $\Delta\omega = \omega_{\mathrm{p}}$. This is in very reasonable agreement with the model, provided that the bandwidth of the fluctuations is determined by the plasma frequency of the Josephson junction detector. For SIS sample, the bandwidth was found to be $0.8\omega_{\mathrm{p}}$ (with $F_3 = 1$).

The lower value of the bandwidth for SIS sample can be attributed to the circuit effects. The finite impedance of the electromagnetic environment leads to an imperfect constant voltage bias of the noise source. The fluctuations of the bias voltage across the noise source lead to a change of the current fluctuations δI and hence affect the current statistics. In our model, the circuit corrections are included phenomenologically in the effective Fano factor F_2^{eff} and the effective bandwidth $\Delta\omega$. In the case when a tunnel junction with a resistance R_N in the shot noise regime is placed in the circuit of impedance Z, the correction to the third moment can be roughly estimated as $\sim Z/(R_N + Z)$. In our experiment the circuit impedance at relevant frequencies $\omega_{\mathrm{p}}/2\pi \sim 50$ GHz is of the order of a vacuum impedance, $Z(\omega_{\mathrm{p}}) \sim 100\ \Omega$. This offers a way to explain the lower bandwidth value for sample SIS with a resistance $R_N = 1.9$ kΩ of the noise source. In sample NIS with $R_N = 15.4$ kΩ the circuit corrections are expected to be much weaker.

3.5   Discussion

We have demonstrated that a Josephson junction (JJ) can be used as a sensitive threshold detector of non-Gaussian current fluctuations in a tunnel junction. We have analyzed the observed shot noise asymmetry assuming that the third order fluctuations result in slow variations of the JJ washboard potential over the bandwidth determined by the plasma frequency of the JJ detector. The influence of the second moment of shot noise is taken into account via a resonant activation in the JJ well which leads to the escape at the effective noise temperature. In addition, our model coincides apart from the numerical prefactor with recently developed theories [43, 44, 45] for a JJ as a noise detector in the classical regime of high temperatures $k_B T \gg \hbar\omega_{\mathrm{p}}$. In a very recent similar experiment by Saclay group [27], the JJ threshold detector in this regime $k_B T \gg \hbar\omega_{\mathrm{p}}$ with a specially engineered circuit was used to detect shot noise asymmetry of a SIS tunnel junction. The experiment showed good agreement with the theory [45], although the measured asymmetry was 50 % larger than predicted. Yet it still appears as a challenging engineering task to design the electromagnetic circuit of the Josephson junction such that no uncertainty remains in the frequency-dependence of the circuit parameters, and thus to use a JJ as an absolute on-chip detector of noise and Fano factors in various mesoscopic conductors.

Chapter 4

Heat relaxation in a BCS superconductor

Heat transport and thermalization at subkelvin temperatures is an important issue in superconducting mesoscopic devices. This chapter focuses on the measurements of quasiparticle energy relaxation in a superconducting island, reported in Paper IV. The obtained results show qualitative agreement with the theory of energy relaxation for clean superconductors, determined by electron-phonon coupling. The quantitative discrepancy suggests the presence of enhanced or additional relaxation processes.

4.1   Quasiparticle relaxation in normal metals and in superconductors

Energy relaxation of hot electrons in normal metals has been studied for several decades and it was measured down to very low temperatures [46, 47, 48, 49, 50, 51]. Typically, in thin metallic films at very low temperatures, the hot electrons interact between themselves via fast electron-electron relaxation, and in the case of quasi-equilibrium they remain at a well defined temperature T_e, which is higher than temperature T_0 of the phonon bath [47, 48]. The rate γ_{e-e} of electron-electron energy relaxation is proportional to temperature as $\gamma_{e-e} \propto \frac{(k_B T)^2}{\hbar E_F}$ [46]. The energy relaxation from hot electrons to cold phonon bath occurs at much longer times. The microscopic process of the energy transfer between electrons and phonons is that the electron with wave vector $\mathbf{k}$ and energy E_k is scattered to state $\mathbf{k}' = \mathbf{k} \pm \mathbf{q}$ with energy $E_{k'}$, absorbing or emitting a phonon with wave vector $\mathbf{q}$ and energy $\epsilon = |E_k - E_{k'}|$. At low temperatures, the electron-phonon relaxation rate depends on temperature as $\gamma_{e-ph} \propto T^3$ for a clean metal, when the electron mean free path ℓ_e is much longer than the thermal phonon wavelength $2\pi/q \sim hv/k_B T$. Here, $v \sim 3-5$ km/s is a typical sound velocity in metals. The electron scattering on impurities, defects and surfaces destroys the single-particle picture of electron-phonon interaction [50]. Consequently in disordered metals, where the electron mean free path is shorter than the wave length of a thermal phonon, the electron-phonon relaxation rate can scale with temperature as $\gamma_{e-ph} \propto T^2$ or T^4, depending on the nature of disorder [50]. The calculations of the net heat flux P_{e-ph} from electrons to phonons for a bulk

clean metal yield the following result [48]:

$$P_{\text{e}-\text{ph}} = \Sigma\Omega(T_e^5 - T_0^5). \tag{4.1}$$

Here, Σ is a material constant [9], and Ω is the volume of the system. This equation gives a good account of the heat flux for most experiments at sub-kelvin temperatures. The observed deviations from T^5 law arise from disorder [49] or reduction in dimensionality [51], when the wave length of a thermal phonon becomes of the order of the sample size.

In superconductors the relaxation processes are much slower than in normal metals, due to the fact that quasiparticle excitations are separated by the superconducting energy gap from the ground state. The relaxation of a quasiparticle with energy $E > \Delta$ in a clean superconductor can be described in a two-step process [52]. First, the quasiparticle relaxes to the state with energy Δ at a certain scattering rate τ_s^{-1}, emitting the phonon(s), whose total energy is $E - \Delta$. The concentration of such quasiparticles with energies $\approx \Delta$ can be large due to high density of states closely above the gap. Second, the quasiparticle recombines with another quasiparticle to form a Cooper pair, emitting the phonon of energy 2Δ. At temperatures well below T_c, the total number of thermally excited quasiparticles in the superconductor is exponentially small: it is proportional to $e^{-\Delta/k_B T}$. Thus, the recombination rate τ_{rec}^{-1} of quasiparticles slows down exponentially at low temperatures. The theoretical calculations of the rates [52, 53] give the following results: $\tau_s^{-1} \propto T^{7/2}$ and $\tau_{\text{rec}}^{-1} \propto T^{1/2}e^{-\Delta/k_B T}$. Hence the recombination is the main mechanism that slows down energy relaxation at lower temperatures. The rates were measured soon after theoretical predictions [52], and the recent experiments [54, 55, 56, 57] at very low temperatures suggest to confirm the exponential behavior of recombination rate down to $T/T_c \simeq 0.2$. At lower temperatures, the relaxation rate saturates due to presently poorly known reasons, possibly due to the disorder, as the latest experiment indicates [57].

Like the recombination rate, the heat flux between quasiparticles and phonons in a BCS superconductor is also expected to be suppressed exponentially at lower temperatures. However, this issue has not been addressed explicitly before. In Paper IV, we presented both experimental and theoretical results which demonstrate the importance of slow thermal relaxation in superconductors.

The theoretical calculations of the quasiparticle-phonon energy flux $P_{\text{e}-\text{ph}}$ for a clean superconductor (derived in paper IV in a similar way to Eq. (4.1) from the quasiclassical theory [58]) yield the suppression of $P_{\text{e}-\text{ph}}$, which is shown in Fig. 4.5 at the end of the chapter where it is compared with the experiment. At low temperatures $T_0 \ll T_e \ll \Delta/k_B$, $P_{\text{e}-\text{ph}} \simeq \frac{64}{63\zeta(5)}\Sigma\Omega T_e^5 e^{-\Delta/k_B T_e}$, which is by a factor $0.98 e^{-\Delta/k_B T_e}$ smaller than that in the normal state (Eq. (4.1) with $T_0 \ll T_e$).

We have studied experimentally quasiparticle energy relaxation in aluminium islands, both in superconducting and normal metal states. First, we discuss the measurements when the island is in a superconducting state.

4.2 Heat relaxation measurements in a superconducting state

Energy relaxation of quasiparticles was investigated by injecting hot electrons into the superconducting island through a small tunnel junction and measuring quasiparticle current using another small SIS junction. The typical sample design and measurement configuration are illustrated in Fig. 4.1.
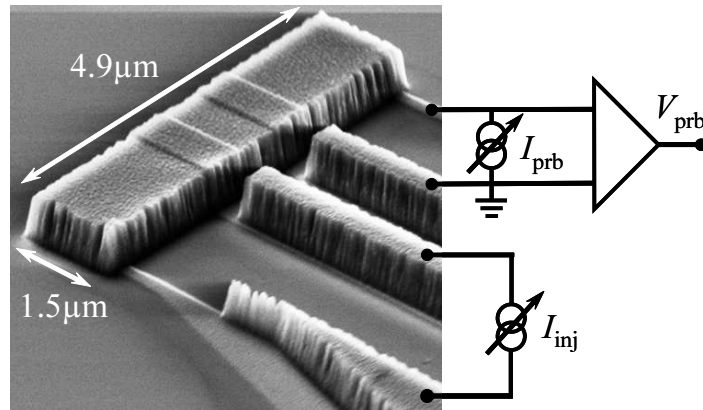
Figure 4.1: Electron micrograph of a sample for relaxation measurements (sample C). The aluminium block is the volume in which energy relaxation is measured. The circuits indicate the injection of hot quasiparticles and probing the island temperature.

The superconducting island is contacted by two small and two large SIS junctions. We have studied three samples (denoted as A, B, and C) with different island dimensions and different tunnel resistances of the junctions. The parameters of the samples are given in Table 4.1.

Table 4.1: Sample dimensions and junction resistances.

Sample	volume (μm^3)	R_1, R_2, R_3, R_4 (kΩ)
A	$21 \times 1.5 \times 0.44$	840, 4, 4, 1160
B	$4.9 \times 1.5 \times 0.44$	760, 5.7, 5.7, 1290
C	$4.9 \times 1.5 \times 0.44$	485, 20, 20, 980

The hot quasiparticles are injected via one of the small tunnel junctions in series with a large one. The injecting current I_{inj} has a floating connection and it is swept in the range of $\simeq 0.5 - 100$ nA, so that a small SIS junction with tunnel resistance $R_T \sim 1$ MΩ is biased into the quasiparticle regime, with voltages $2\Delta < eV_{inj} < 500\Delta$ across it. Because of the large asymmetry between small and large junctions, essentially all the power is injected by the small junction. Since the junction is biased into a resistive state, it behaves as a normal metal (NIN) tunnel junction, for which the power is divided evenly between the two junction electrodes. The power deposited into the island equals $P = I_{inj}V_{inj}/2$ and it is in the range $\simeq 0.1$ pW - 10 nW. We assume that

the absorbed power in the island in the steady state equals the power transferred to the phonons, emitted by the quasiparticles. The quasiparticle current I is detected by measuring the current-voltage characteristic of the second pair of junctions, biased at voltages $0 < eV < 2\Delta$. We observe the quasiparticle current of a small junction, the large junction remained in the superconducting state. We neglect the power input due to the probing voltage V, since it is orders of magnitude smaller than that due to the injection. We have also carried out measurements with two small junctions in series as injectors and two large junctions as quasiparticle current probes, which gave essentially identical results.

In the measurements we aim at realizing the situation when the hot electrons injected into the island are in quasi-equilibrium at a temperature T_e decoupled from the heat bath which consists of thermal phonons at much lower temperature T_0. The validity of these assumptions is discussed below.

The results of the measurements and the theoretically calculated IV curves using

$$eR_T I = \int dE n_{T_e}(E - eV) n_{T_0}(E)[f_{T_e}(E - eV) - f_{T_0}(E)], \qquad (4.2)$$

are presented in Fig. 4.2. In Eq. (4.2), it is assumed that quasiparticles have Fermi distributions f_{T_e} in the island and f_{T_0} in the leads, and $n_{T_e}(E - eV)$ and $n_{T_0}(E)$ are the superconducting densities of states in the island and in the leads, correspondingly.

First, we measured equilibrium IV curves of the probing junction at different bath temperatures $T_0(= T_e)$, without current injection, see Fig. 4.2(b). The calculated equilibrium IV curves from Eq. (4.2) with $T_e = T_0$ are shown in Fig. 4.2(a). The plateaus on the IV curves at voltages $0 < eV < 2\Delta$ emerge due to the quasiparticle current I. The value of I at $eV = \Delta$ for different temperatures T_0/T_c is plotted in Fig. 4.2(c). The agreement between the data (triangles) and theory (lines) is good down to $T_0/T_c \simeq 0.25$. Here, $T_c \simeq 1.45$ K is the measured critical temperature. The temperature increase due to the low bias voltage V is assumed to be vanishingly small. At lower temperatures, the data saturates. There are at least two possible reasons for this: 1) the quasiparticle current becomes lower than a supercurrent, and 2) there is excess current due to the presence of quasiparticle states within the superconducting gap[1]. Yet the data can be fitted using a pair-breaking parameter γ. We focus our analysis to the range $0.3 < T_e/T_c < 1$ where no such fit parameter is needed.

---

[1]The inelastic scattering of quasiparticles on the impurities and defects in a superconductor [59] leads to the finite quasiparticle density of states n_s within the superconducting gap and makes n_s to be smeared in a real experimental situation. This smearing can be modelled by including a phenomenological pair-breaking parameter γ into the expression for n_s:

$$n_s(E) = \left| \mathrm{Re} \frac{E + i\gamma\Delta}{\sqrt{(E + i\gamma\Delta)^2 - \Delta^2}} \right|. \qquad (4.3)$$

The parameter γ is often used to determine the quality of the tunnel barriers, and for the junctions in the present work its values are typically in the range $10^{-4}...10^{-3}$.
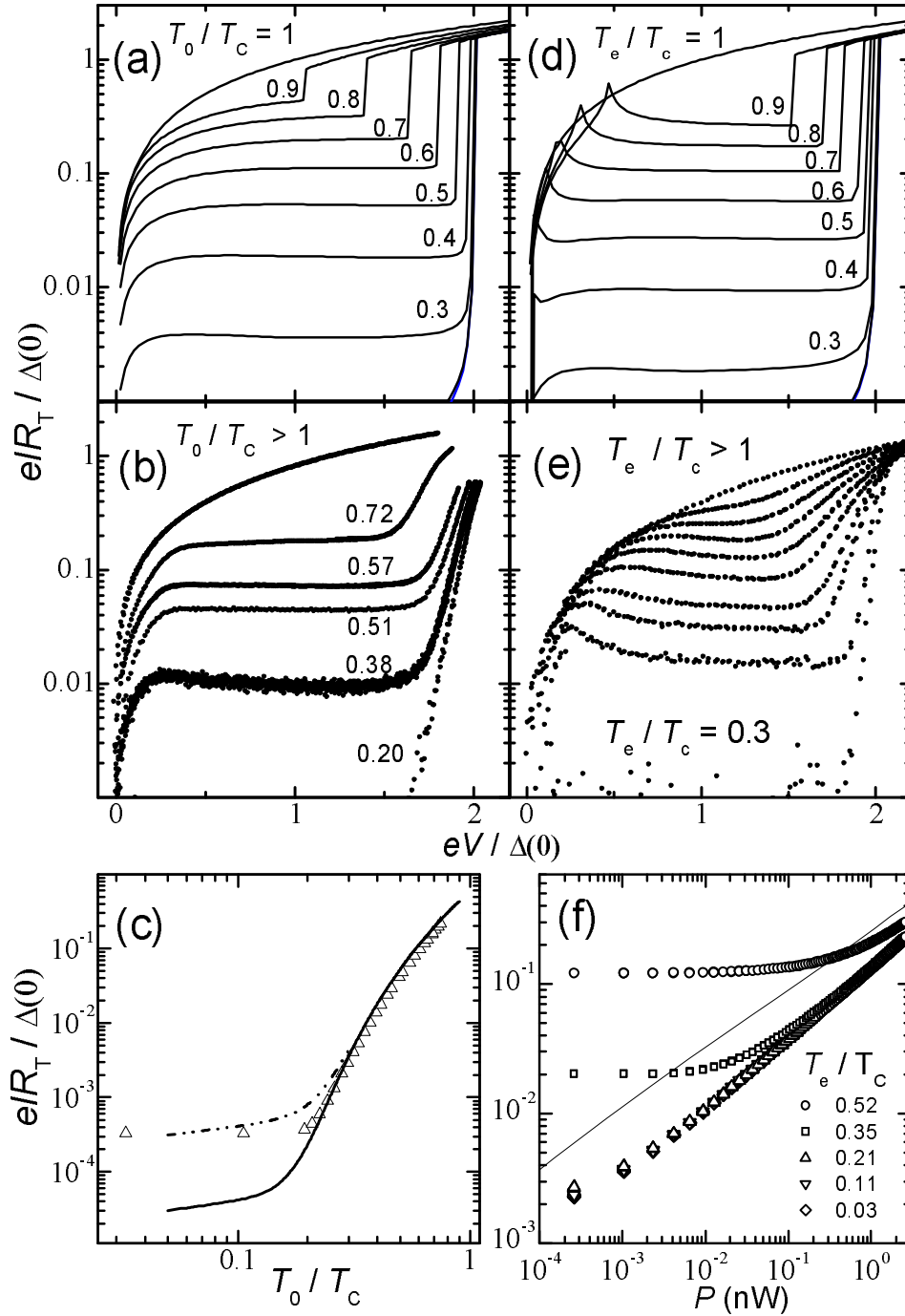
Figure 4.2: Tunnel currents for a superconductor in equilibrium and quasi-equilibrium. (a) Theoretical and (b) experimental IVs of a junction at several bath temperatures when $T_e = T_0$ (Sample A). (c) Theoretical and experimental currents at $eV = \Delta$ (Sample B). The two theory lines correspond to pair breaking parameters $\gamma = 10^{-3}$ (upper curve) and $\gamma = 10^{-4}$ (lower curve). (d) Calculated IVs when the leads (at $T_0 = 50$ mK) and the island have different temperatures, $T_e \neq T_0$. (e) The measured IVs under a few injection conditions (Sample C). (f) The current in Sample A on the plateau between the initial peak and the rise of the current at the conduction threshold around $2\Delta/e$. The theoretical prediction for the lowest T_0 is shown by the solid line. The value of Δ at zero temperature is 200 ± 5 μeV, and $T_c = 1.45 \pm 0.03$ K.

Next, we discuss the case when the power has been injected into the island. Figure 4.2(d) shows the calculated IV curves of the probe junction, assuming that only the island temperature T_e is elevated, and the leads of the probe junctions remain at $T_0 = 0.05 T_c$. A peak in the IVs arises at $eV = \Delta(T_e) - \Delta(T_0)$ due to the difference of superconducting gaps of the island and the leads. Figure 4.2(e) shows the corresponding measured curves at various levels of injected power at $T_0 = 50$ mK. The data 4.2(e) resemble the behavior of the calculated curves 4.2(d), yet the peak at the gap difference and the strong quasiparticle onset at the gap voltage are smeared, which could originate from a noisy electromagnetic environment [60] (attributing it to the smearing due to the sub-gap states yields unreasonably large γ parameter). The measurements of current injection were performed at several bath temperatures. The minimum of the current (Fig. 4.2e) in the plateau regime between the peak and the quasiparticle onset as a function of injected power is plotted in Fig. 4.2(f) for different bath temperatures. In a wide temperature range $T_0 = 30 - 380$ mK, (0.02-0.26)T_c, the quasiparticle current is independent of bath temperature T_0 and depends only on the injected power. This indicates that the phonons remain at much lower temperatures T_0 and all the quasiparticles are created only due to the current injection. This is also a typical case in normal metals when the hot electrons at low temperatures are thermally decoupled from the phonon bath [48]. Therefore, in what follows we compare our experimental results with the theory at the base phonon temperature $T_0 = 50$ mK $\ll T_e$.

To compare the measured results with the theory, the minimum quasiparticle current on plateau in Fig. 4.2(e) is converted to temperature T_e by comparing it to temperature dependent minimum plateau current of the theoretical IV curves in Fig. 4.2(d). For the data at $T_e/T_c \gtrsim 0.9$, when the minimum vanishes and the plateau becomes tilted, we use the current at the value of V where the curvature of the IV changes the sign in the interval $\Delta < eV < 2\Delta$. Consequently, the uncertainty in determining T_e above $0.9 T_c$ is larger. The reduced quasiparticle temperature T_e/T_c as a function of injected power is plotted in Figure 4.3. The power is normalized by that at T_c, to present data from different samples on the same footing. For samples A, B and C, $P(T_c) = 14$ nW, 3 nW, and 3 nW, respectively. The data on the three samples are mutually consistent — the normalized injected power is independent of the island volume indicating that the electron-phonon is the main energy relaxation mechanism, consistent with the theoretical discussion. The theoretical result for the heat flux P_{e-ph} is shown by the solid line.

The heat flux through the (probing) junction is given by the equation $P(V) = (e^2 R_T)^{-1} \int (E - eV) n_{T_e}(E - eV) n_{T_0}(E)[f_{T_0}(E) - f_{T_e}(E - eV)]dE$. Its value is low and almost constant over a wide range of voltages within the gap region, and therefore it can be neglected under most experimental conditions. Yet, to test this, we varied the resistances of the large tunnel junctions by a factor of five between samples A and C, without a significant effect on the results. Thus the junctions are opaque enough not to conduct heat from the island into the leads.
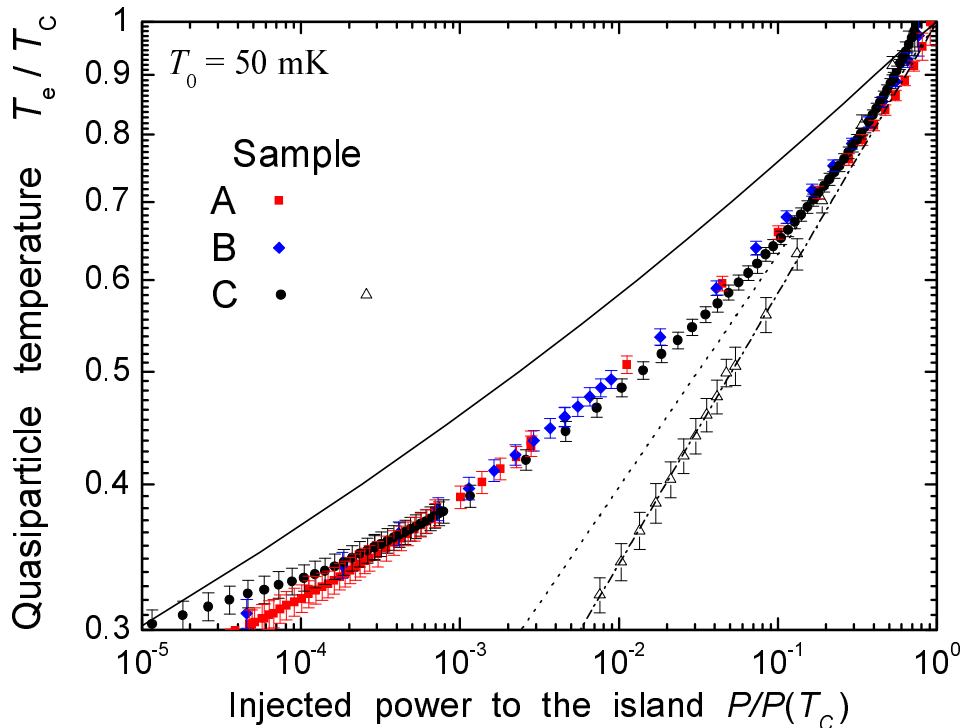
Figure 4.3: Energy relaxation from theory and experiment. The data in the superconducting state are from sample A (squares), B (diamonds), and C (circles). The error bars indicate the temperature uncertainty which arises when determining the temperature either from the minimum current (from the current where the IV curvature changes the sign at $T_e \gtrsim 0.9T_c$), or from the current at $eV = \Delta$ on the plateaus in Fig. 4.2(e). The open triangles are the result of the measurements of sample C in the normal state. The solid line shows the theoretical result for the superconducting state. The dotted line indicates $P/P(T_c) = (T_e/T_c)^5$, and the dashed-dotted line $P/P(T_c) = (T_e/T_c)^{4.3}$.

4.2.1 Conditions for quasi-equilibrium

The deviation from quasi-equilibrium distribution of hot quasiparticles is determined on one hand by the rate $\eta = (4e^2N(0)\Omega R_T)^{-1}$ [61, 62], at which the electrons are injected through the tunnel junction of a resistance R_T into the volume Ω. The effects of non-equilibrium quasiparticles were observed in the early experiments with large junctions [63, 64] and later with Nb-AlOx-Nb junctions [61, 65, 66], where large injection currents and low resistive junctions were used. This led to non-equilibrium quasiparticle distributions due to high current injection rates $\sim 10^8$ s^{-1} [61]. In the present experiment, much lower currents I_{inj} are injected into the superconducting island with a large volume Ω through small and high resistive tunnel junctions, with slow injection rates: $\eta \sim 10$ s^{-1} and $\eta \sim 10^3$ s^{-1} for small and large junctions, correspondingly. Yet the large junctions have a much lower voltage drop $< 0.04V_{inj}$. For aluminium at temperatures $T \sim T_c$, the electron-electron relaxation rate $\gamma_{e-e} \sim 10^8...10^9$ s^{-1} [9, 67, 16], and the electron-

phonon relaxation rate $\gamma_{e-ph}= (\tau_s^{-1}+\tau_{rec}^{-1})$ is $\sim 10^6...10^7$ s^{-1}. Thus the requirement of quasi-equilibrium $\eta \ll \gamma_{e-e}, \gamma_{e-ph}$ is fulfilled in our experiment.

Very recently Kopnin *et al.* [68] presented a theory where the distribution of quasi-particles created by high-voltage injection can deviate considerably from thermal, so that at energies $E \sim eV \gg k_B T_e$ the electron-phonon relaxation rate can become larger than the electron-electron relaxation rate. In this case, the quasiparticles with $E \sim eV$ emit high-energy phonons, which carry away most of the deposited energy from the sample into the substrate, due to good thermal contact with the island. The energy transferred to thermal phonons (emitted by quasiparticles with energies $\sim k_B T_e$) is then much smaller than the total deposited energy. Such a deviation from equilibrium can be roughly estimated by comparing the tail of thermal distribution function $\sim e^{-\Delta/k_B T_e}$ with a non-equilibrium correction $\phi(\Delta)$ to the quasiparticle distribution function [68]. For not very high voltages $eV \sim 10^2\Delta$, the correction can be expressed as $\phi(E) \sim \frac{\eta}{\gamma_{e-e}} \left(\frac{\Delta}{E}\right)^4 \left(\frac{eV_{inj}}{\Delta}\right)^2$. For the parameters in our experiment, $\phi(\Delta) \sim 10^{-7} \left(\frac{eV_{inj}}{\Delta}\right)^2 \lesssim 10^{-3}$, and $e^{-\Delta/k_B T_e} \gtrsim 10^{-2} > \phi(\Delta)$ for $T_e \gtrsim 0.3 T_c$. Thus, even for the injection voltages $eV_{inj} \sim 100\Delta$ used in the experiment, the deviations from quasi-equilibrium are small.

Also, the shape of the IV curves in figure 4.2, the exponential dependence of the plateau current vs power, and the consistency between the three samples with different parameters (different injection voltages by factor of three under the same conditions) support further that quasi-equilibrium is a good approximation in our experiment.

We have also assumed that the non-equilibrium distribution of phonons does not play a role in our experiments. However, during the quasiparticle recombination mostly phonons with energy 2Δ are created. If these phonons do not decay faster than quasi-particles recombine, the phonon distribution is not an equilibrium one [69]. If that would be the case in our experiment, a smaller power than expected by theory would be needed to raise the temperature of the quasiparticle population, and the data would lie above the theoretical line, which is contrary to our observation. Therefore, we can state that non-equilibrium phonons are not the reason for the observed discrepancy between the experiment and theory.

4.3   Heat relaxation measurements in a normal metal state

We measured heat relaxation in the normal state in one of the samples (sample C) as well. Superconductivity was suppressed by applying a magnetic field of about 120 mT. The temperature of hot electrons on the island was deduced by measuring the partial Coulomb blockade (CB) signal [12]. The dependence of the junction conductance on the temperature in the equilibrium case $T_e = T_0$ is discussed in Chapter 1. In the quasi-equilibrium case, when the temperature on the two sides of the junction is unequal,

$T_0 \ll T_e$, the conductance is given by

$$\frac{G^{\text{quasi}}}{G_T} = 1 - \frac{E_C}{2k_B T_e} \frac{1}{\cosh^2(eV/4k_B T_e)}, \tag{4.4}$$

as was presented in paper IV. The depth of the conductance minimum at $V = 0$ is $\Delta G/G_T = E_C/2k_B T_e$ which is 50% larger than that in the equal temperature case. The full width is $V_{1/2}^{\text{quasi}} = 4\ln(3 + 2\sqrt{2})k_B T_e/e$. This is about 65% of the equal-temperature value, $V_{1/2}^{\text{eq}} \simeq 10.88 k_B T_e/e$ [12].

The two large junctions were used for probing the electron temperature, and the small ones for power injection. The estimated charging energy of the large junctions is $E_C/k_B \simeq 20$ mK, which is ideal for a measurement of the island temperature via partial Coulomb blockade. The value $V_{1/2}^{\text{eq}}$ yielded a good quantitative agreement with the equilibrium temperature data over the whole range of the experiment. The three measured conductance curves of the probing junctions under injection are shown in Fig. 4.4. The low base temperature permits the use of the expression of $V_{1/2}^{\text{quasi}}$ above to extract T_e in the range displayed in Fig. 4.3. Power law type behavior can be observed over the whole temperature range $0.3T_c < T_e \lesssim T_c$. The data approach those of the superconducting state near $T_c \simeq 1.45$ K, as expected. The power law for $P_{\text{e-ph}}$ can be approximated by $T_e^{4.3}$ (dashed line) instead of T_e^5 (dashed-dotted line) of Eq. 4.1, with a deviation of the same sign with respect to the theory as in the superconducting state.
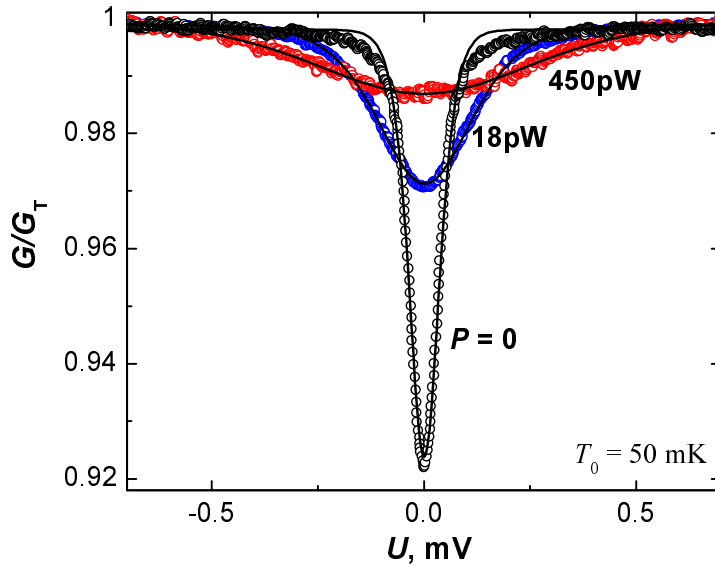
Figure 4.4: The three Coulomb peaks measured in the normal state under different levels of power injection: the solid lines are theoretical fits to them.

We have also estimated the temperature gradient of the aluminium island in the normal state at $T_e \approx T_c$ due to quasiparticle diffusion by solving numerically the heat

diffusion equation

$$\frac{d}{dx}\left(\kappa_n \frac{dT_e(x)}{dx}\right) = \Sigma_{Al} T_e^5(x), \tag{4.5}$$

where x is a coordinate along the island of a length ℓ with the cross-section $A = 1.5 \times 0.44$ μm^2, and the boundary conditions are $T_e'(\ell) = 0$ and $T_e(\ell) = T_c$. Here, $\Sigma_{Al} = 0.3 \times 10^{-9}$ $WK^{-5}m^{-3}$ is the material constant for aluminium [9], the heat conductivity $\kappa_n = L_0 T_c/\rho$ is determined using the Wiedemann-Franz law, $L_0 \simeq 2.4 \cdot 10^{-8}$ $W\Omega K^{-2}$ is the Lorenz number, and $\rho = (0.9 - 1) \times 10^{-8}$ Ωm is the measured resistivity of the aluminium bar in the normal state. The obtained temperature gradient along the island ($\ell = 21$ μm) for sample A is about 5%, and for shorter islands ($\ell = 4.9$ μm) in samples B and C it is only about 0.3%, and therefore the heat diffusion is negligibly small in our experiments.

4.4   Discussion

The theoretical and experimental results on the suppression of the electron-phonon heat flux in the superconducting state with respect to that in normal state are shown in Fig. 4.5 in a form of $\alpha(T_e/T_c)$. The factor $\alpha(T_e/T_c) = P_s/P_N$ is deduced as the ratio of the
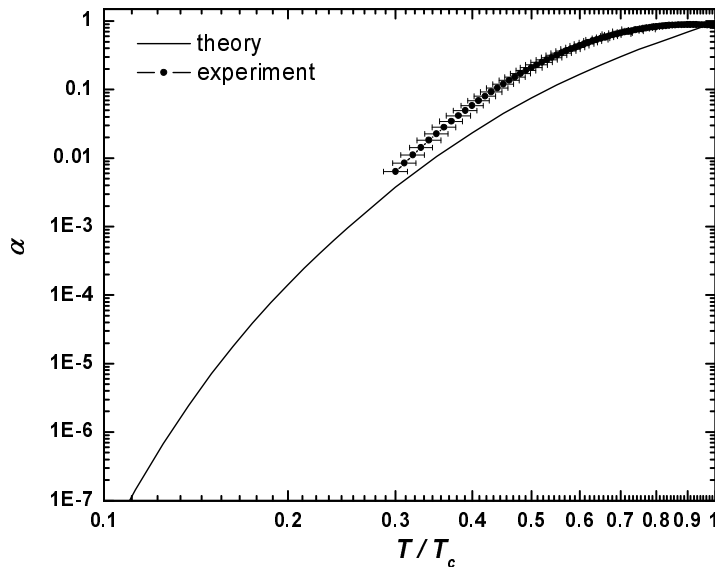
Figure 4.5: Theoretical and experimental results on the suppression of the electron-phonon heat flux in the superconducting state.

powers P_s in the superconducting and P_N in the normal state (Fig. 4.3). The data demonstrate that electron-phonon coupling in a superconductor is weaker than in the normal state, by two orders of magnitude at $T_e/T_c = 0.3$. But, like in the experiments on quasiparticle relaxation time in a superconductor [54, 55, 56], the relaxation is faster than that from the theory [52, 58]. This observation could suggest that the relaxation both

in the superconducting and in the normal state might be sensitive to the microscopic quality and the impurity content of the particular film [50]. The effect of impurities on the electron-phonon relaxation may become pronounced when the thermal phonon wavelength $2\pi/q = hv/k_B T_e$ is comparable with the electron mean free path ℓ_e. The estimation of mean free path for aluminium[2] yields $\ell_e \sim 20$ nm, which gives $ql \lesssim 1$ at $T_e \lesssim 1$ K.

Our experiments, performed on three samples with quite different parameters, yielded essentially identical results when normalized by the island volume. Therefore we believe that issues like thermal gradients, non-equilibrium, and heat leaks through tunnel contacts have only a minor influence on the results. The data thus yield the intrinsic energy relaxation of quasiparticles in the superconducting and in the normal state. Our experimental data follow qualitatively the presented theoretical model. Quantitatively, our observations suggest the presence of an additional relaxation process, which may arise from the impurities and disorder, as it is briefly discussed in Summary section.

---

[2]The mean free path is estimated from Drude formula $l = v_F \frac{m}{\rho n e^2}$, where $m = 9.1 \times 10^{-31}$ kg is the electron mass, and the electron density for aluminium is $n = 18 \times 10^{22}$ cm^{-3} [70].

Chapter 5

Electronic refrigeration at the quantum limit

In this chapter, we discuss the experiment of paper V on quantum limited heat transport mediated by electromagnetic radiation. This photon heat relaxation mechanism was recently pointed out to be relevant for metallic nanostructures at very low temperatures [71], and it was observed not long after by Meschke *et al.* [72]. In the present experiment, we show that such a radiative heat transport can be used for a distant electronic refrigeration of small metallic islands. We also observe and analyze the temperature crossover between quasiparticle and electromagnetic heat transport in a superconductor. In addition, our observations are important for the realization of a so-called Brownian electron refrigerator, which was recently proposed in [73].

5.1 Quantum limit of heat transport via a single channel

It is known that the maximum of heat conductance of a single channel is determined by the universal quantum of thermal conductance $G_Q = \pi k_B^2 T/(6\hbar)$ irrespectively of the statistics of heat carrying particles [74, 75, 76]. Here, a single channel is associated with a one of the variables used to describe the heat flow [74]. The maximum limit for the single-channel heat flow can be derived from general physical principles, e.g., considering the bound for the entropy flow[1] through a single heat channel between two particle reservoirs [76].

The quantum limit of heat transport was experimentally observed for phonons in thin suspended insulating bridges [77], for electrons in a semiconducting one-dimensional wire [78], and for photons in a superconducting circuit with two microscopic metallic resistors

---

[1]The net flows of entropy $\dot{S} = \dot{S}_1 - \dot{S}_2$ and heat $\dot{Q} = \dot{Q}_1 - \dot{Q}_2$ in the channel between reservoirs 1 and 2 are related as $\dot{S}^2 \leqslant \frac{1}{3\hbar}\pi k_B^2 \dot{Q}$, which follows from the bound estimations of the integrals over the energy distributions of the particles. In case of massless bosons, phonons or photons (as the latter one in our experiment), when the chemical potentials of the two reservoirs are zero, we have for each reservoir $\dot{Q}_{1,2} = \frac{1}{12\hbar}\pi(k_B T_{1,2})^2$ and $\dot{S}_{1,2} = \frac{1}{6\hbar}\pi k_B^2 T_{1,2}$. According to the second law of thermodynamics, the entropy tends to increase always (approaching maximum value at equilibrium), $\dot{S}_{1,2} \geqslant \dot{Q}_{1,2}/T_{1,2}$, from where the upper limit for the single-channel heat flow can be deduced: $\dot{Q}_{1,2} \leqslant \frac{1}{3\hbar}\pi(k_B T_{1,2})^2$. The upper bound of single-channel heat conductance can be obtained from the tighter bound inequality $\dot{S}^2 \leqslant \frac{\pi k_B^2}{3\hbar}\dot{Q}\left(\frac{T_1 - T_2}{T_1 + T_2}\right)$, analytically derived for fermions [76].

[72]. In the latter case of photons, the single heat channel can be associated with the polarization of a one-dimensional electromagnetic wave in a planar superconducting strip line [74, 79]. Such a radiative heat exchange between two resistors connected with dissipation free line was originally discussed already by Nyquist back in 1928 [80], who derived expressions for the power of thermal noise produced by the resistor in classical and quantum regimes. The results for the electrical circuits in these two limits can be summarized as follows. For macroscopic electrical circuits at high temperatures, when the thermal frequency $\omega_T = k_B T/\hbar$ is much larger than the characteristic circuit frequency ω_c, the power of the radiative heat exchange is determined by the product of the average energy $k_B T$ per each degree of freedom (an electromagnetic mode at a single frequency $\omega/2\pi$) and the circuit bandwidth, since the thermal noise is cut-off at the circuit frequency ω_c. For microscopic low temperature circuits as in our experiment, the noise is cut-off at thermal frequencies which are much lower than the circuit frequencies, the average energy per each mode is partitioned according to the Planck distribution. The net power of electromagnetically exchanged energy between the resistors R_1 and R_2 with corresponding temperatures T_1 and T_2 can be written as [71]

$$P_\nu = \int_0^\infty \frac{d\omega}{2\pi} \frac{4R_1 R_2}{|Z_t(\omega)|^2} \hbar\omega \left(\frac{1}{e^{\hbar\omega/k_B T_2} - 1} - \frac{1}{e^{\hbar\omega/k_B T_1} - 1} \right), \tag{5.1}$$

where $Z_t(\omega)$ is the frequency dependent total series impedance of the circuit. For electronic metallic nanostructures, this radiative heat relaxation mechanism becomes dominant at low temperatures when electron-phonon and normal electronic heat conduction are sufficiently weak [71].

In the experiment by Meschke *et al.* [72], the two resistors were connected with superconducting lines interrupted by SQUIDs, and due to that the circuit was not perfectly matched and the full quantum of thermal conductance was not reached. In the experiment described in paper V, we have studied the heat transport between the resistors in a matched circuit, which allowed to observe the radiative heat flow directly at the limit of one quantum. We showed that the impedance matching is indeed relevant for the observation of the effect — we found no radiative heat exchange in the sample with a mismatched circuit.

5.2 Measured samples. Electrical and thermal models

To observe quantum heat transport and to demonstrate the relevance of impedance matching, we carried out measurements on two samples, with a matched and a mismatched circuit. The electron micrographs of the samples and their equivalent electrical schemes are shown in Figs. 5.1 and 5.2. In the matched sample, the two identical gold-palladium islands (resistors) are connected with the superconducting lines into a loop, whereas in the mismatched sample the islands are connected with a single superconducting line. In the mismatched sample, one of the islands was made about 3 times shorter
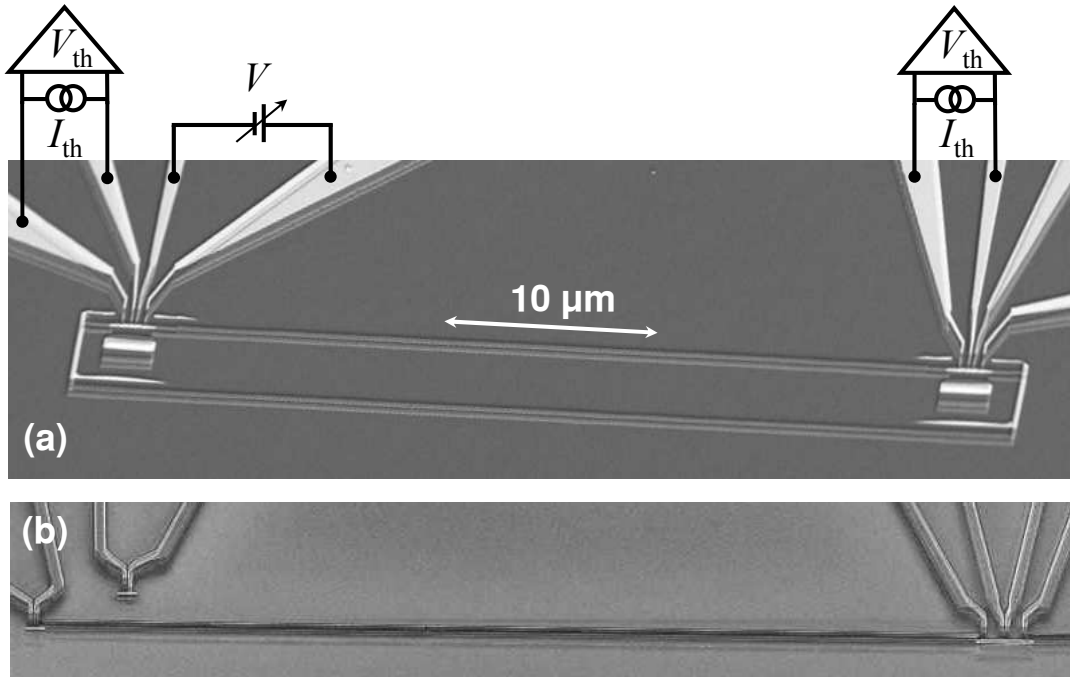
Figure 5.1: Electron micrographs of the samples with the matched (a) and mismatched (b) circuits. In panel (a), the schematic electric connections indicate the voltage sweeping through one pair of NIS junctions and the temperature measurements of the islands.
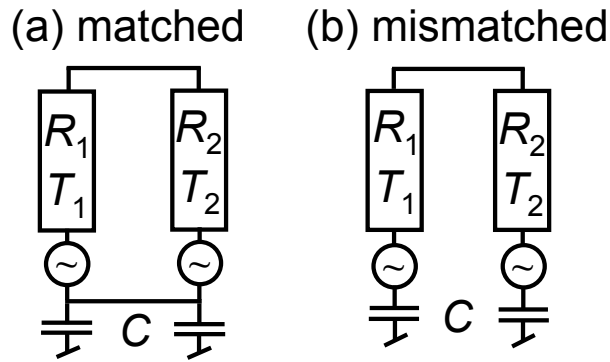
Figure 5.2: Equivalent electrical circuits of the matched (a) and mismatched (b) samples.

than the other one, in order to further increase mismatching.[2] The distance ℓ between the islands in both samples was about 50 μm. The wavelength of thermal photons $\frac{hc}{k_B T}$ is several centimeters at temperatures 0.1 - 0.5 K, and we can consider equivalent lumped electrical circuits of our samples. Thus, in the matched sample, due to the circuit shorted by the loop, the voltage noise emitted by the resistors generates noise current in the loop

---

[2]The volume of each island in the matched sample is $\Omega = 3 \times 0.2 \times 0.02$ μm^3. In the mismatched sample, the volumes of islands 1 and 2 are $\Omega_1 = 3 \times 0.18 \times 0.02$ μm^3 and $\Omega_2 = 1 \times 0.18 \times 0.02$ μm^3.

leading to heat exchange between the two islands. In the mismatched circuit, the circuit is closed only by small capacitance of the NIS junctions to the ground, and the radiative heat exchange is suppressed. According to Eq. (5.1), the radiative net heat fluxes in the matched $P_\nu^{\mathrm{m}} = \frac{\pi k_B^2}{12\hbar}(T_2^2 - T_1^2)$ and the mismatched $P_\nu^{\mathrm{mism}} \simeq \frac{\pi^3 k_B^2}{30\hbar}(T_2^2 - T_1^2)(k_B TRC/\hbar)^2$ circuits scale as $P_\nu^{\mathrm{mism}}/P_\nu^{\mathrm{m}} \simeq \frac{2\pi^2}{5}(\omega_T/\omega_c)^2$ at low temperatures, $\omega_T \ll \omega_c$. For the parameters in the experiment, $R \simeq 200\ \Omega$, $C \simeq 10$ fF, the electromagnetic power flow in the matched circuit is estimated to be about $10^2 - 10^3$ times stronger as compared to that in the mismatched case at temperatures $0.3 - 0.1$ K.

To study heat transport between the islands, we perturbed and measured electronic temperatures of the islands using NIS tunnel junctions, which are contacting each island in the middle. One pair of NIS junctions was used to refrigerate or heat one of the islands by sweeping DC-voltage V across the junctions. At voltages smaller than twice the superconducting gap $\Delta \simeq 0.2$ meV of aluminium, $eV < 2\Delta$, the junctions work as a SINIS-refrigerator [9, 17, 18], removing hot electrons from the island through the tunnel barriers into the superconducting leads, which results in a reduction of the electronic temperature of the island. The refrigeration effect is maximal at $eV \simeq 2\Delta$. To probe the temperature of the refrigerated island, the second pair of NIS junctions is used as a thermometer by applying a small DC current I_{th} through it, and by measuring the corresponding temperature dependent voltage V_{th}. Another similar SINIS-thermometer probes the temperature T_2 of the second island. When the applied voltage V through the SINIS-refrigerator is zero, the measured voltage $V_{\mathrm{th}}(V = 0)$ provides the thermometer calibration against the bath temperature T_0 varied in the range $50 - 500$ mK. The electronic temperature of the islands is then obtained from the fit of the dependence of T_0 on $V_{\mathrm{th}}(V = 0)$, shown in Fig. 5.3. At $V = 0$ the electronic temperature coincides with the bath temperature down to $T_0 = 120$ mK. At lower temperatures, the thermometer signal saturates due to overheating of the electrons by residual parasitic noise via the electrical leads. The estimated parasitic power at 100 mK is $\sim \Sigma_{\mathrm{AuPd}}\Omega T^5 \sim 0.5$ fW. The thermometers have individual floating DC bias sources and do not cause excessive heating or cooling of the islands due to the low bias current, $I_{\mathrm{th}} \simeq 0.001\Delta/eR_T$, used.

The thermal model that accounts for our set-up and observations is shown in Fig. 5.4. The resistors exchange energy at power P_ν through the electromagnetic channel, and, in parallel, at power P_s, due to quasiparticle heat conduction through the superconducting line. The latter contribution is significant at higher temperatures but diminishes exponentially towards low temperatures $k_B T_0 \ll \Delta$ [81]. We analyze the contribution of quasiparticle heat flux quantitatively with the heat diffusion equation

$$\frac{d}{dx}\left(-\kappa_s \frac{dT}{dx}\right) = \alpha(T_0)\Sigma_{\mathrm{Al}}[T_0^5 - T^5(x)], \tag{5.2}$$

assuming that the superconducting line has the temperature profile $T(x)$ with boundary conditions $T(0) = T_2$ and $T(\ell) = T_1$. Here, x is the coordinate along the line ($x = 0$ corresponds to the contact to island 2, $x = \ell$ to that to island 1). Factor $\alpha(T_0)$ (see
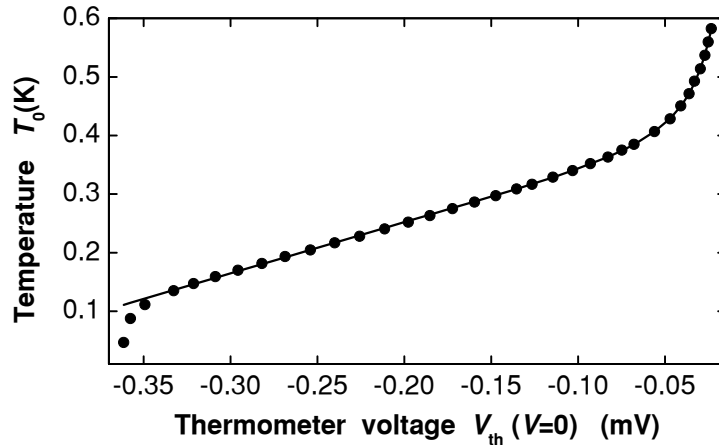
Figure 5.3: SINIS-thermometer calibration for the matched sample, measured with the thermometer current $I_{th} \simeq 14$ pA. The line shows the fit to data points, which is linear below 300 mK.
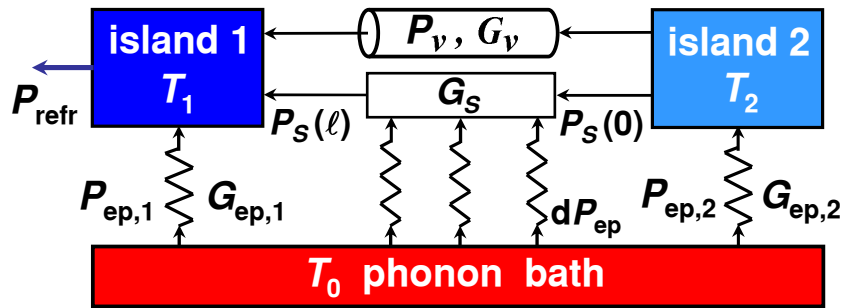
Figure 5.4: The thermal model illustrates electromagnetic (P_ν, G_ν) and quasiparticle (P_s, G_s) heat conduction through the superconducting line between the two islands. The islands are thermally coupled to the phonon bath with the heat fluxes $P_{ep,1}$ and $P_{ep,2}$. The weak electron-phonon coupling of the superconducting line to the thermal bath is denoted by dP_{ep}. The arrows show the direction of the heat flow for temperatures $T_1 < T_2 < T_0$.

Chapter 4) defines the suppression of electron-phonon coupling in the superconducting line with respect to that in the normal state [82], and $\Sigma_{Al} \simeq 0.3 \cdot 10^9$ WK^{-5}m^{-3} is a material constant for aluminium [9]. The heat flux $P_s(0) = -\kappa_s A T'(0)$ to island 1, and the heat flux $P_s(L) = -\kappa_s A T'(\ell)$ from island 2 are determined through temperature gradients $T'(0)$ and $T'(\ell)$ at the ends of the superconducting line with cross-sectional area $A = 200 \times 25$ nm^2. Here, $\kappa_s = \gamma(T_0)\kappa_n$ is the heat conductivity of the superconducting line [81], suppressed by a factor [3] $\gamma(T_0)$ with respect to heat conductivity $\kappa_n = L_0 T(x)/\rho$ in the normal state. Here, $\rho =$(1.4 - 1.5)$\times 10^{-8}$ Ωm is the measured resistivity of the aluminium line. The electrons in each resistor of volume Ω_i exchange energy with the

---

[3]$\gamma(T_0) = \frac{3}{2\pi^2} \int_{\Delta(T_0)/k_B T_0}^{\infty} \frac{t^2 dt}{\cosh^2(t/2)}$.

substrate, i.e., with the thermal bath at temperature T_0 via electron-phonon coupling at the rate $P_{\mathrm{ep},i} = \Sigma_{\mathrm{AuPd}}\Omega_i(T_0^5 - T_i^5)$ [47, 48], where $\Sigma_{\mathrm{AuPd}} \simeq (2-4)\cdot 10^9$ WK^{-5}m^{-3} is obtained from the measurements. Here, we assume that phonons in the islands are well thermalized with the substrate phonons, since thermal Kapitza resistance is negligibly small at the interface between two phonon systems. This is a typical case for thin films at such low temperatures ~ 0.3 K [48], when the wavelength of thermal phonons $\simeq 1$ μm is large as compared to the film thickness (20 nm). Island 1 can be SINIS-refrigerated (or heated) with the corresponding power P_{refr}. Also, we neglect phonon heat transport based on experimental results detailed below. The steady-state of the system is then described by the energy balance equations

$$P_{\mathrm{refr}} - P_\nu - P_s(\ell) - P_{\mathrm{ep},1} = 0$$
$$P_\nu + P_s(0) - P_{\mathrm{ep},2} = 0. \tag{5.3}$$

For the quantitative analysis of the heat transport, we solved numerically Eq. (5.2) together with Eqs. (5.3) to obtain the relative temperature change of island 2 with respect to that of island 1, $\Delta T_2/\Delta T_1 \equiv (T_2 - T_0)/(T_1 - T_0)$. For small temperature differences, neglecting the electron-phonon coupling in the superconductor, we can linearize the different contributions in Eqs. (5.3) and obtain a particularly simple expression for $\Delta T_2/\Delta T_1$:

$$\frac{\Delta T_2}{\Delta T_1} = \frac{G_\nu + G_s}{G_\nu + G_s + G_{\mathrm{ep},2}}. \tag{5.4}$$

Here, the photon coupling G_ν is expected to be equal to G_Q for the matched sample and for the mismatched sample it is suppressed by a large factor as discussed above. The electron-phonon conductance is given by $G_{\mathrm{ep},2} = 5\Sigma_{\mathrm{AuPd}}\Omega_2 T_0^4$, and G_s denotes the ordinary heat conductance by quasiparticles in the superconducting line.

5.3   Measurement results

The results of the measurements are shown in Figure 5.5. We observed the quantum limited refrigeration of the second island in the matched sample and found no such effect in the mismatched one. The dependence of the two island temperatures ΔT_1 and ΔT_2 on the bias voltage V for the two samples are shown in Figs. 5.5(a) and 5.5(b) at few bath temperatures T_0.

For a quantitative comparison of the remote refrigerating effect, we plot the maximal temperature drops of the two islands at the optimal bias point $eV \simeq 2\Delta$ against the bath temperatures $T_0 = 0.1 - 0.5$ K in Fig. 5.5(c) and 5.5(d), and also the corresponding relative temperature drops $\Delta T_2/\Delta T_1$ in Figs. 5.5(e) and 5.5(f). Clearly, in the sample with the matched circuit, the temperature of the probing island 2 tends to follow the temperature behavior of the main island 1, and at temperatures below 300 mK $\Delta T_2/\Delta T_1$ increases rapidly, as can be expected based on strong electromagnetic coupling. In
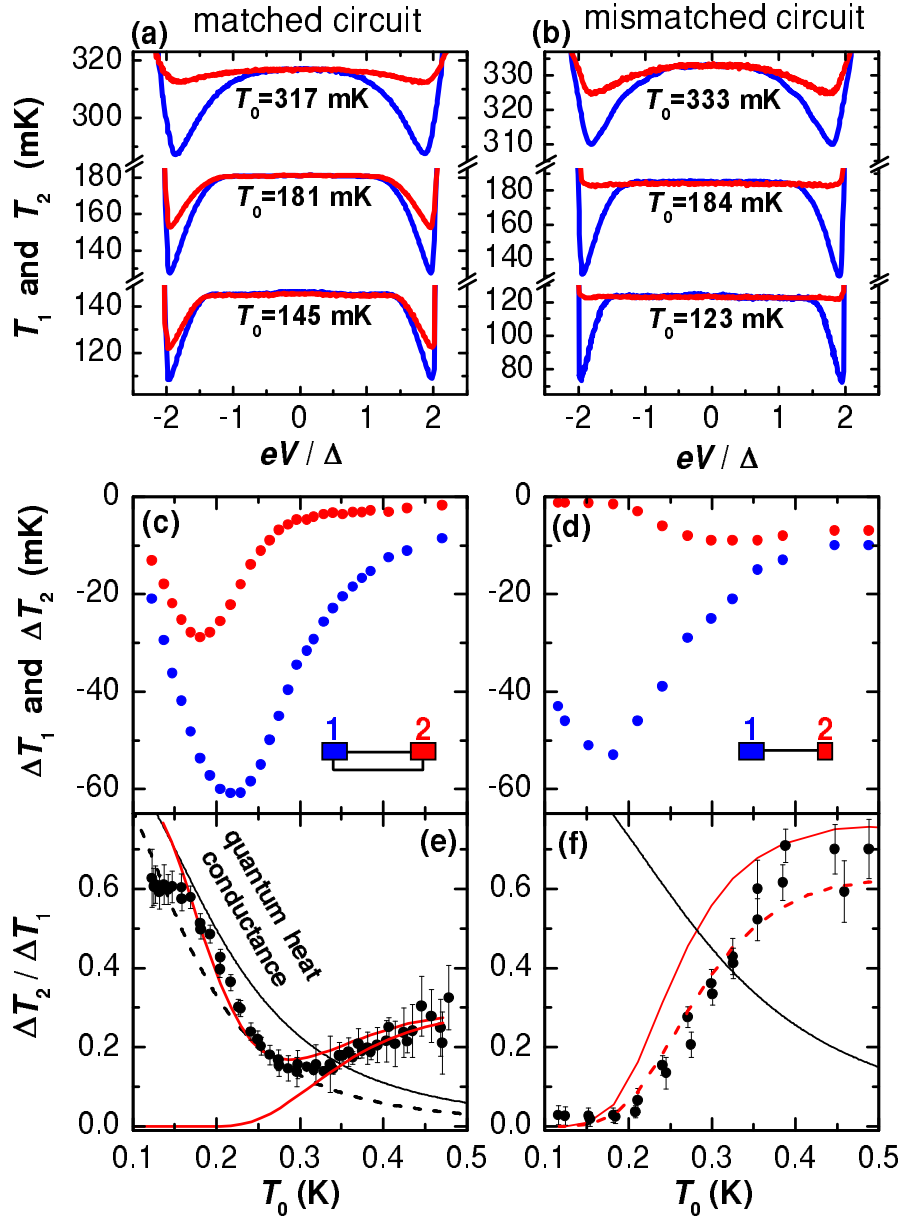
Figure 5.5: Measured data of matched (a, c, e) and mismatched B (b, d, f) samples, and calculated results of the thermal model. (a), (b): Measured island temperatures T_1 (blue line) and T_2 (red line) vs. bias voltage V at three bath temperatures T_0. (c), (d): Absolute temperature changes ΔT_1 (blue dots) and ΔT_2 (red dots) measured at $T_0 =$120 - 500 mK. (e), (f): Relative temperature change $\Delta T_2/\Delta T_1$ at 120 - 500 mK are shown by the black dots. The error bars show the standard deviation arising from the temperature calibration. (e), (f): The black lines are obtained from the linearized thermal model. The red lines are the results of the numerical thermal model. The solid lines are calculated with $\Sigma_{\mathrm{AuPd}} = 2 \cdot 10^9$ WK^{-5}m^{-3} and the dashed lines with $\Sigma_{\mathrm{AuPd}} = 4 \cdot 10^9$ WK^{-5}m^{-3}.

contrast, the refrigeration of the remote island in the mismatched sample is suppressed at low temperatures, $\Delta T_2 / \Delta T_1$ vanishes due to weak photonic coupling.

We note that the cooling power of the NIS refrigerator itself is a non-monotonic function of temperature, it has a maximum at $T \simeq 0.25 \Delta / k_B$ in the simplest case of an ideal tunnel barrier, decreasing both at lower and higher temperatures [9]. Also, at low temperatures ~ 100 mK, the cooling power is limited by several factors like nonidealities in tunnel barriers (for instance, pin holes), possible non-equilibrium effects in normal metal island and superconducting leads, Andreev current, and sub-gap quasiparticle states, which all lead to heating of the island. Due to these reasons, we observe non-monotonic temperature behavior of the ordinary NIS refrigeration and the saturation of $\Delta T_2 / \Delta T_1$ for the matched sample at low temperatures $\lesssim 150$ mK.

The rise of $\Delta T_2 / \Delta T_1$ for the matched sample at temperatures below 300 mK in Fig. 5.5(e) is in agreement with the simple linearized thermal model: the data lie between the solid and dashed black lines, obtained from Eq. (5.4) assuming full quantum conductance $G_\nu = G_Q$ and vanishing quasiparticle conductance $G_s = 0$. Alternatively, the dashed black line can be obtained from Eq. (5.4) with $G_\nu = 0.5 G_Q$ and $\Sigma_{\mathrm{AuPd}} = 2 \cdot 10^9$ WK^{-5}m^{-3}, since only the photonic G_ν and the electron-phonon $G_{\mathrm{ep},2}$ coupling contribute to the relative temperature drop $\Delta T_2 / \Delta T_1$ when $G_s = 0$. Based on these results we conclude that the matching in this sample is close to ideal and the refrigeration is limited by the quantum of thermal conductance. This effect is absent in the mismatched sample: for reference we show the black line in Fig. 5.5(f) with $G_\nu = G_Q$ and $G_s = 0$.

The quantitative behaviour of $\Delta T_2 / \Delta T_1$ at high temperatures $T_0 \gtrsim 300$ mK is not universal and depends on sample parameters. For the matched sample, $\Delta T_2 / \Delta T_1$ is non-monotonic — it has a minimum around 300 mK, which we attribute to the crossover between electromagnetic and quasiparticle heat transport. Also, at $T_0 \gtrsim 300$ mK, the remote island of the mismatched sample is refrigerated more than that in the matched one. This is because of stronger thermalization of the matched sample with larger island 2, and since there are, due to the deposition technique, extra normal (AuPd) shadows covering the vertical parts of the aluminium looped line (see Fig. 5.1a). In the mismatched sample, the normal shadow is not in contact with the superconducting line, which further enhances the quasiparticle mediated refrigeration. For the matched sample, the data over the full temperature range are accounted for by the upper red line in Fig. 5.5(e), obtained from the numerical analysis with $P_\nu = P_\nu^{\mathrm{A}}$ and $\Sigma_{\mathrm{AuPd}} = 2 \cdot 10^9$ WK^{-5}m^{-3}. To fit the data for the matched sample in the diffusion regime $T_0 \gtrsim 300$ mK, we added a fitting parameter $\alpha_N = 0.6$ to the factor α: $\alpha \rightarrow \alpha + \alpha_N$. The parameter α_N describes stronger thermalization of the superconducting line. The lower red line in Fig. 5.5(e), calculated with $\alpha_N = 0.6$ and with no photonic heat exchange ($P_\nu = 0$), shows the quasiparticle contribution for comparison. For the mismatched sample, the numerically obtained red curves of quasiparticle conduction are shown in Fig. 5.5(f). The dashed red curve shows good agreement with the data. The uncertainty in the quantitative comparison between the model and data arises from only approximately

known parameters of electron-phonon coupling for gold-palladium and aluminium thin films.

In both samples the islands are strongly heated at voltages $eV > 2\Delta$ due to the injection of hot quasiparticles. An additional thermometer, located near island 2, but not connected to it, was monitoring phonon temperature on the substrate. It showed negligibly weak temperature response as compared to the thermometers of islands 1 and 2. This supports our thermal model, which assumes that phonons provide a good thermal bath and that the observed heat exchange between the resistors occurs due to quasiparticles and electromagnetic radiation. This is a natural conclusion due to the very weak electron-phonon coupling at low temperatures.

In the analysis, we have also neglected the voltage fluctuations on the island due to the shot noise in the NIS junctions, since these fluctuations are small as compared to the equilibrium voltage noise of the island resistors. This is because the junctions are biased with a low voltage, of the order of the superconducting gap, $eV \simeq \Delta$ ($\simeq 2.3$ K for aluminium), and the tunnel resistance $R_T \simeq 19$ kΩ of the junctions is about two orders of magnitude larger than the island resistance $R \simeq 200$ Ω. The estimation of the voltage noise density on the island due to the shot noise yields $S_{shot}^V < \frac{eV}{R_T}R^2$, whereas the equilibrium voltage noise is $S_{eq}^V \sim 2\hbar\omega_T R$. Thus, the contribution of the shot noise is weak: $\frac{S_{shot}^V}{S_{eq}^V} < \frac{eV}{k_B T}\frac{R}{2R_T} \sim 0.02 - 0.1$ for temperatures $T = 0.5 - 0.1$ K.

5.4   Discussion and prospects for Brownian electron refrigerator

To summarize, we demonstrated electronic refrigeration of a metallic micro-island at the quantum limit, when the heat transport occurs via the electromagnetic radiation governed by the quantum of thermal conductance. We showed that the impedance matching of the circuit is vitally important for the observation of such an effect. Our measurements and model suggest that even galvanically separated resistors can be refrigerated by such a mechanism. This could be an option for the refrigeration of dissipative micro-components and noise suppression in sensitive quantum devices, such as SQUIDs. Also, we observed how two different heat conduction mechanisms in a superconductor — those by quasiparticles and by photons — dominate in different temperature regimes. These observations are also significant for the superconductor-based devices including micro-bolometers and calorimeters. The issues of circuit matching and quasiparticle heating are relevant for the realization of a recently proposed Brownian electron refrigerator [73], when the normal metal island in the NIS junction can be refrigerated by thermal noise of a hot resistor radiated via superconducting leads. For the experimental implementation of such a device, the resistor has to be heated up so that the voltage fluctuations are of appropriate magnitude to remove hot electrons out from the normal metal through the tunnel barrier into a superconductor. The noise of the resistor will be strongly coupled

to NIS junction if the circuit impedance is matched. The quasiparticle heating of the superconducting line has to be suppressed to avoid parasitic heating of the island, which can be done, e.g., by thermalizing the line to the surrounding cold bath. Yet another way to eliminate quasiparticle heating issue would be to use a capacitive coupling between the junction and the resistor.

Summary and outlook

The experiments reviewed in this Thesis showed that tunnel junctions can be used as versatile devices to study charge and heat transport in mesoscopic systems.

A Josephson junction is demonstrated to be a sensitive noise detector to resolve higher order current fluctuations in a wide bandwidth of about 50 GHz, determined by the plasma frequency of the junction. The second moment of shot noise is detected via resonant activation of the Josephson junction. The observed shot noise asymmetry is described with the model of non-resonant response of the Josephson junction to the third order fluctuations at subplasma frequencies. With a careful tailoring of the surrounding electromagnetic circuit, a Josephson junction has a potential to be used as an absolute detector of noise and current statistics in various mesoscopic conductors.

The experiments on electron heat relaxation showed the importance of slow electron-phonon relaxation in the superconducting state at low temperatures, in qualitative agreement with the theory for clean superconductors. Quantitatively the energy flux exceeds the theoretical predictions both in the superconducting and in the normal state, suggesting enhanced or additional still-to-be-investigated relaxation processes, which may arise from microscopic imperfections, impurities and surfaces. One of the extra relaxation mechanisms can be related to the presence of magnetic impurities in a superconductor, which give rise to the formation of electron states within the gap that are localized in the vicinity of the impurity atom [83]. A quasiparticle can be trapped into such a sub-gap state, and then recombine with another quasiparticle from the continuum spectrum above the gap resulting in an enhanced recombination, as the recent theoretical result shows [84]. In other words, magnetic impurities can act as recombination centers providing fast thermalization and changing the temperature dependence of quasiparticle relaxation rates. Also, the recent experimental result [57] on measuring quasiparticle lifetimes in superconducting Ta and Al films suggests that the recombination at low temperatures can be also enhanced due to disorder, most likely involving unpaired magnetic surface spins. Thus further theoretical analysis and experiments are required to elucidate the details of the microscopic mechanisms which lead to an enhanced quasiparticle relaxation.

The radiative electronic refrigeration of a metallic micro-island was demonstrated in a superconducting circuit with a cooling power limited by the universal quantum of heat conductance. It was shown that matching the circuit impedance is necessary for the observation of such radiative heat transport. Also, the crossover between electromagnetic

and quasiparticle heat transport mechanisms in a superconductor was observed and analyzed. The demonstrated effect brings relevant information for the realization of a Brownian electron refrigerator [73], whose operating principle relies on the propagation of thermal radiation in a superconducting circuit at sub-kelvin temperatures.

Finally, regarding the topic of fluctuations and heat transport in mesoscopic physics, one can foresee experiments to study both equilibrium temperature fluctuations [85, 86] and full statistics of energy transfer in nanoscale systems out of equilibrium to observe the effects of temperature fluctuations beyond Gaussian regime, as it has been theoretically considered in Refs. [87, 88].

Bibliography

[1] Y. M. Blanter and M. Büttiker, *Shot Noise in Mesoscopic Conductors*, Phys. Rep. **336**, 1 (2000).

[2] L. Levitov and G. Lesovik, *Charge Distribution in Quantum Shot Noise*, JETP letters **58**, 225 (1993).

[3] L. S. Levitov, H. Lee, and A. Y. Yakovetz, *Electron counting statistics and coherent states of electric current*, J. Math. Phys. **37**, 4845 (1996).

[4] B. Reulet, J. Senzier, and D. E. Prober, *Environmental Effects in the Third Moment of Voltage Fluctuations in a Tunnel Junction*, Phys. Rev. Lett. **91**, 196601 (2003).

[5] J. Bardeen, L. N. Cooper, and J. R. Schrieffer, *Theory of Superconductivity*, Phys. Rev. **108**, 1175 (1957).

[6] B. Huard, *Ph.D. thesis* (Université Pierre and Marie Curie, Paris VI, 2006).

[7] I. Giaever and K. Megerle, *Study of Superconductors by Tunneling*, Phys. Rev. **122**, 1101 (1961).

[8] V. Ambegaokar and V. Baratoff, *Tunneling Between Superconductors*, Phys. Rev. Lett. **10**, 486 (1963).

[9] F. Giazotto, T. T. Heikkila, A. Luukanen, A. M. Savin, and Jukka P. Pekola, *Opportunities for Mesoscopics in Thermometry and Refrigeration: Physics and Applications*, Rev. Mod. Phys. **78**, 217 (2006).

[10] J. G. Simmons, *Generalized Formula for the Electric Tunnel Effect between Similar Electrodes Separated by a Thin Insulating Film*, J. Appl. Phys. **34**, 1793 (1963).

[11] K. Gloos, R. S. Poikolainen, and J. P. Pekola, *Wide-range thermometer based on the temperature-dependent conductance of planar tunnel junctions*, Appl. Phys. Lett. **77**, 2915 (2000).

[12] J. P. Pekola, K. P. Hirvi, J. P. Kauppinen, and M. A. Paalanen, *Thermometry by Arrays of Tunnel Junctions*, Phys. Rev. Lett. **73**, 2903 (1994).

[13] Sh. Farhangfar, K. P. Hirvi, J. P. Kauppinen, J. P. Pekola, J. J. Toppari, D. V. Averin and A. N. Korotkov, *One dimensional arrays and solitary tunnel junctions in the weak coulomb blockade regime: CBT thermometry*, J. Low Temp. Phys. **108**, 191 (1997).

[14] J. P. Pekola, T. Holmqvist, and M. Meschke, *Primary Tunnel Junction Thermometry*, Phys. Rev. Lett. **101**, 206801 (2008).

[15] T. Holmqvist, M. Meschke, and J. P. Pekola, *Influence of Environment on Tunneling Thermometry*, J. Low Temp. Phys. **154**, 172 (2009).

[16] J. Kivioja, *Ph. D. Thesis, Mesoscopic Superconducting Tunnel Junction Devices* (Helsinki University of Technology, Finland, 2005).

[17] M. Nahum, T. M. Eiles, and J. M. Martinis, *Electronic Micro-Refrigerator Based on a Normal-Insulator-Superconductor Tunnel Junction*, Appl. Phys. Lett. **65**, 3123 (1994).

[18] M. M. Leivo, J. P. Pekola, and D. V. Averin, *Efficient Peltier Refrigeration by a Pair of Normal Metal/Insulator/Superconductor Junctions*, Appl. Phys. Lett. **68**, 1996 (1996).

[19] A. B. Zorin, *The thermocoax cable as the microwave frequency filter for single electron circuits*, Rev. Sci. Instr. **66**, 4296 (1995).

[20] A. H. Steinbach, J. M. Martinis, and M. H. Devoret, *Observation of hot-electron shot noise in a metallic resistor*, Phys. Rev. Lett. **76**, 3806 (1996).

[21] K. E. Nagaev, *Influence of electron-electron scattering on shot noise in diffusive contacts*, Phys. Rev. B **52**, 4740 (1995).

[22] Y. V. Nazarov, *Quantum Noise in Mesoscopic Physics* (NATO Science Series in Mathematics, 1st ed., Kluwer, 2003).

[23] *Quantum Information and Decoherence in Nanonsystems, Proceedings of the 39th Recontres de Moriond* (eds. D. Ch. Gattli, M. Sanquer, and J. T. T. Van, La Thuile, Italy, 2004).

[24] F. Wu, T. Tsuneta, R. Tarkiainen, D. Gunnarsson, T.-H. Wang, and P. J. Hakonen, *Shot noise of a multiwalled carbon nanotube field effect transistor*, Phys. Rev. B **75**, 125419 (2007).

[25] Y. Bomze, G. Gershon, D. Shovkun, L. S. Levitov, and M. Reznikov, *Measurement of Counting Statistics of Electron Transport in a Tunnel Junction*, Phys. Rev. Lett. **95**, 176601 (2005).

[26] R. K. Lindell, J. Delahaye, M. A. Sillanpää, T.T. Heikkilä, E. B. Sonin, and P. J. Hakonen, *Observation of Shot-Noise-Induced Asymmetry in the Coulomb Blockaded Josephson Junction*, Phys. Rev. Lett. **93**, 197002 (2004).

[27] Q. Le Masne, H. Pothier, Norman O. Birge, C. Urbina, D. Esteve, *Asymmetric Noise Probed with a Josephson Junction*, Phys. Rev. Lett. **102**, 067002 (2009).

[28] S. Gustavsson, R. Leturcq, B. Simovi, R. Schleser, T. Ihn, P. Studerus, K. Ensslin, D. C. Driscoll, and A. C. Gossard, *Counting statistics of single electron transport in a quantum dot*, Phys. Rev. Lett. **96**, 076605 (2006).

[29] S. Gustavsson, R. Leturcq, T. Ihn, K. Ensslin, M. Reinwald, and W. Wegscheider, *Measurements of higher-order noise correlations in a quantum dot with a finite bandwidth detector*, Phys. Rev. B **75**, 075314 (2007).

[30] G. Gershon, Yu. Bomze, E. V. Sukhorukov, and M. Reznikov, *Detection of Non-Gaussian Fluctuations in a Quantum Point Contact*, Phys. Rev. Lett. **101**, 016803 (2008).

[31] J. Tobiska and Y. V. Nazarov, *Josephson Junctions as Threshold Detectors for Full Counting Statistics*, Phys. Rev. Lett. **93**, 106801 (2004).

[32] J. P. Pekola, *Josephson Junction as a Detector of Poissonian Charge Injection*, Phys. Rev. Lett. **93**, 206601 (2004).

[33] B. Reulet, *Higher Moments of Noise* (Les Houches Summer School of Theoretical Physics, Session LXXXI, Nanophysics: Coherence and Transport. NATO ASI, Amsterdam: Elsevier, 2005).

[34] J. Salo, F. W. J. Hekking, and J. P. Pekola, *Frequency-dependent current correlation functions from scattering theory*, Phys. Rev. B **74**, 125427 (2006).

[35] W. Belzig, *Full Counting Statistics in Quantum Contacts*, Lect. Notes Phys. **658**, 123 (2005).

[36] M. H. Devoret, D. Esteve, J. M. Martinis, A. Cleland and J. Clarke, *Resonant activation of a Brownian particle out of a potential well: Microwave-enhanced escape from the zero-voltage state of a Josephson junction*, Phys. Rev. B **36**, 58 (1987).

[37] J. M. Kivioja, T. E. Nieminen, J. Claudon, O. Buisson, F. W. J. Hekking, and J. P. Pekola, *Observation of Transition from Escape Dynamics to Underdamped Phase Diffusion in a Josephson Junction*, Phys. Rev. Lett. **94**, 247002 (2005).

[38] V. M. Krasnov, T. Bauch, S. Intiso, E. Hürfeld, T. Akazaki, H. Takayanagi, and P. Delsing, *Collapse of Thermal Activation in Moderately Damped Josephson Junctions*, Phys. Rev. Lett. **94**, 157002 (2005).

[39] J. Männik, S. Li, W. Qiu, W. Chen, V. Patel, S. Han, and J. E. Lukens, *Crossover from Kramers to phase-diffusion switching in moderately damped Josephson junctions*, Phys. Rev. B **71**, 220509 (2005).

[40] J. P. Pekola, T. E. Nieminen, M. Meschke, J. M. Kivioja, A. O. Niskanen, and J. J. Vartiainen, *Shot-Noise-Driven Escape in Hysteretic Josephson Junctions*, Phys. Rev. Lett. **95**, 197004 (2005).

[41] T. Ojanen and T. T. Heikkilä, *Quantum transitions induced by the third cumulant of current fluctuations*, Phys. Rev. B **73**, 020501(R) (2006).

[42] J. T. Peltonen, *Master Thesis, Josephson Junctions as Detectors of non-Gaussian Noise* (Helsinki University of Technology, Finland, 2008).

[43] J. Ankerhold, *Detecting Charge Noise with a Josephson Junction: A Problem of Thermal Escape in Presence of Non-Gaussian Fluctuations*, Phys. Rev. Lett. **98**, 036601 (2007).

[44] E. Sukhorukov and A. N. Jordan, *Stochastic Dynamics of a Josephson Junction Threshold Detector*, Phys. Rev. Lett. **98**, 136803 (2007).

[45] H. Grabert, *Theory of a Josephson junction detector of non-Gaussian noise*, Phys. Rev. B **77**, 205315 (2008).

[46] V. F. Gantmakher, *Electron-phonon scattering in metals*, Rep. Prog. Phys. **37**, 317 (1974).

[47] M. L. Roukes, M. R. Freeman, R. S. Germain, R. C. Richardson, and M. B. Ketchen, *Hot Electrons and Energy Transport in Metals at Millikelvin Temperatures*, Phys. Rev. Lett. **55**, 422 (1985).

[48] F. C. Wellstood, C. Urbina, and J. Clarke, *Hot-Electrons effects in Metals*, Phys. Rev. B **49**, 5942 (1994).

[49] E. Chow, H. P. Wei, S. M. Girvin, and M. Shayegan, *Phonon Emission from a 2D Electron Gas: Evidence of Transition to the Hydrodynamic Regime*, Phys. Rev. Lett. **77**, 1143 (1996).

[50] A. Sergeev and V. Mitin, *Electron-phonon interaction in disordered conductors: Static and vibrating scattering potentials*, Phys. Rev. B **61**, 6041 (2000).

[51] J. T. Karvonen and I. J. Maasilta, *Influence of Phonon Dimensionality on Electron Energy Relaxation*, Phys. Rev. Lett. **99**, 145503 (2007).

[52] S. B. Kaplan, C. C. Chi, D. N. Langenberg, J. J. Chang, S. Jafarey, and D. J. Scalapino, *Quasiparticle and phonon lifetimes in superconductors*, Phys. Rev. B **14**, 4854 (1976).

[53] M. Y. Reizer, *Electron-phonon relaxation in pure metals and superconductors at very low temperatures*, Phys. Rev. B **40**, 5411 (1989).

[54] P. K. Day, H. G. LeDuc, B. A. Mazin, A. Vayonakis, and J. Zmuidzinas, *A broadband superconducting detector suitable for use in large arrays*, Nature **425**, 817 (2003).

[55] A. G. Kozorezov, J. K. Wigmore, A. Peacock, A. Poelaert, P. Verhoeve, R. den Hartog, and G. Brammertz, *Local trap spectroscopy in superconducting tunnel junctions*, Appl. Phys. Lett. **78**, 3654 (2001).

[56] R. Barends, S. van Vliet, J. J. A. Baselmans, S. J. C. Yates, J. R. Gao, and T. M. Klapwijk, *Quasiparticle Relaxation in Optically Excited High-Q Superconducting Resonators*, Phys. Rev. Lett. **100**, 257002 (2008).

[57] R. Barends, S. van Vliet, J. J. A. Baselmans, S. J. C. Yates, J. R. Gao, and T. M. Klapwijk, *Enhancement of quasiparticle recombination in Ta and Al superconductors by implantation of magnetic and nonmagnetic atoms*, Phys. Rev. B **79**, 020509 (2009).

[58] N. B. Kopnin, *Theory of Nonequilibrium Superconductivity* (Clarendon Press, Oxford, 2001).

[59] R. C. Dynes, J. P. Garno, G. B. Hertel, and T. P. Orlando, *Tunneling Study of Superconductivity near the Metal Insulator Transition*, Phys. Rev. Lett. **53**, 2437 (1984).

[60] G. L. Ingold and Yu. V. Nazarov, ed. H. Grabert and M. H. Devoret, *Single Charge Tunneling, Chap. 2* (NATO ASI Series Vol. 294, Plenum Press, New York, 1992).

[61] D. A. Ryndyk, *Nonequilibrium Josephson effect in systems of tunnel superconducting junctions and in layered superconductors*, JETP letters **89**, 975 (1999).

[62] J. Voutilainen, T. T. Heikkilä, and N. B. Kopnin, *Nonequilibrium phenomena in multiple normal-superconducting tunnel heterostructures*, Phys. Rev. B **72**, 054505 (2005).

[63] B. I. Miller and A. H. Dayem, *Relaxation and recombination times of quasiparticles in superconducting Al thin films*, Phys. Rev. Lett. **44**, 486 (1980).

[64] I. Iguchi and D. N. Langenberg, *Diffusive Quasiparticle Instability toward Multiple-Gap States in a Tunnel-Injected Nonequilibrium Superconductor*, Phys. Rev. Lett. **44**, 486 (1980).

[65] M. G. Blamire, E. C. G. Kirk, J. E. Evetts, and T. M. Klapwijk, *Extreme critical-temperature enhancement of Al by tunneling in Nb/AlOx/Al/AlOx/Nb tunnel junctions*, Phys. Rev. Lett. **66**, 220 (1991).

[66] I. P. Nevirkovets, M. G. Blamire, and J. E. Evetts, *Observation of extreme enhancement of superconducting properties of the middle Nb/Al layer in double-barrier tunnel structures*, Low Temp. Phys. **21**, 963 (1995).

[67] B. Shinozaki and L. Rinderer, *Temperature and randomness dependence of the pair-breaking parameter in superconducting aluminum films*, J. Low Temp. Phys. **73**, 267 (1988).

[68] N. Kopnin, Y. M. Galperin, J. Bergli, and V. M. Vinokur, *Nonequilibrium electrons in tunnel structures under high-voltage injection*, arXiv:0905.1210.

[69] A. Rothwarf and B. N. Taylor, *Measurement of Recombination Lifetimes in Superconductors*, Phys. Rev. Lett. **19**, 27 (1967).

[70] N. W. Ashcroft and N. D. Mermin, *Solid State Physics* (W. B. Saunders Co, USA, 1976).

[71] D. R. Schmidt, R. J. Schoelkopf, and A. N. Cleland, *Photon Mediated Thermal Relaxation of Electrons in Nanostructures*, Phys. Rev. Lett. **93**, 045901 (2004).

[72] M. Meschke, W. Guichard, and J. P. Pekola, *Single-Mode Heat Conduction by Photons*, Nature **444**, 187 (2006).

[73] J. P. Pekola and F. W. J. Hekking, *Normal-Metal-Superconductor Tunnel Junction as a Brownian Refrigerator*, Phys. Rev. Lett. **98**, 210604 (2007).

[74] J. B. Pendry, *Quantum Limits to the Flow of Information and Entropy*, J. Phys. A **16**, 2161 (1983).

[75] L. G. C. Rego and G. Kirczenow, *Fractional Exclusion Statistics and the Universal Quantum of Thermal Conductance: A Unifying Approach*, Phys. Rev. B **59**, 13080 (1999).

[76] M. P. Blencowe and V. Vitelli, *Universal Limits on Single Channel Information, Entropy and Heat Flow*, Phys. Rev. A **62**, 052104 (2000).

[77] K. Schwab, E. A. Henriksen, J. M. Worlock, and M. L. Roukes, *Measurement of the Quantum of Thermal Conductance*, Nature **404**, 974 (2000).

[78] O. Chiatti, J. T. Nicholls, Y.Y. Proskuryakov, N. Lumpkin, I. Farrer, and D. A. Ritchie, *Quantum Thermal Conductance of Electrons in a One-Dimensional Wire*, Phys. Rev. Lett. **97**, 056601 (2006).

[79] T. Ojanen and T. T. Heikkilä, *Photon Heat Transport in Low Dimensional Nanostructures*, Phys. Rev. B **76**, 073414 (2007).

[80] H. Nyquist, *Thermal Agitation of Electric Charge in Conductors*, Phys. Rev. **32**, 110 (1928).

[81] J. Bardeen, G. Rickayzen, and L. Tewordt, *Theory of the Thermal Conductivity of Superconductors*, Phys. Rev. **113**, 982 (1959).

[82] A. V. Timofeev, C. P. García, N. B. Kopnin, A. M. Savin, M. Meschke, F. Giazotto, and J. P. Pekola, *Recombination-Limited Energy Relaxation in a Bardeen-Cooper-Schrieffer Superconductor*, Phys. Rev. Lett. **102**, 017003 (2009).

[83] A. V. Balatsky, I. Vekhter, and Jian-Xin Zhu, *Impurity-induced states in conventional and unconventional superconductors*, Rev. Mod. Phys. **78**, 373 (2006).

[84] A. G. Kozorezov, A. A. Golubov, J. K. Wigmore, D. Martin, P. Verhoeve, R. A. Hijmering, and I. Jerjen, *Inelastic scattering of quasiparticles in a superconductor with magnetic impurities*, Phys. Rev. B **78**, 174501 (2008).

[85] L. Landau and E. Lifshitz, *Statistical Physics* (Pergamonn press, New York, 1980).

[86] T. C. P. Chui, D. R. Swanson, M. J. Adriaans, J. A. Nissen, and J. A. Lipa, *Temperature Fluctuations in the Canonical Ensemble*, Phys. Rev. Lett. **69**, 3005 (1992).

[87] M. Kindermann and S. Pilgram, *Statistics of Heat Transfer in Mesoscopic Circuits*, Phys. Rev. B **69**, 155334 (2004).

[88] T. T. Heikkilä and Y. Nazarov, *Statistics of Temperature Fluctuations in an Electron System out of Equilibrium*, Phys. Rev. Lett. **102**, 130605 (2009).